# Lung injury shifts pulmonary capillary endothelial cells towards regeneration-associated Lrg1+ subpopulations with delayed dynamics in aged mice

Marin Truchi[1*], Grégoire Savary[2*], Hugo Cadis[1], Kevin Lebrigand[1], Alberto Baeri[1], Arun Lingampally[3], Cédric Girard-Riboulleau[1], Célia Scribe[1], Virginie Magnone[1], Marie-Jeanne Arguel[1], Clémentine de Schutter[2], Marine Gautier-Isola[1], Julien Fassy[1], Roger Rezzonico[1], Romain Larrue[2], Olivier Pluquet[2], Michael Perrais[2], Véronique Hofman[4], Charles-Hugo Marquette[5], Paul Hofman[4], Andreas Günther[6,7], Nicolas Ricard[8], Pascal Barbry[1], Sylvie Leroy[1,5], Christelle Cauffiez[2], Saverio Bellusci[3], Georges Vassaux[1], Nicolas Pottier[2*] and Bernard Mari[1*#]

***1*** *Université Côte d'Azur, CNRS UMR7275, IPMC, FHU-OncoAge, IHU RespiERA, Valbonne, France*
***2*** *Univ. Lille, CNRS, Inserm, CHU Lille, Institut Pasteur de Lille, UMR9020 CNRS - U1277 Inserm - CANTHER, Lille, France.*
***3*** *Excellence Cluster Cardio-Pulmonary System, German Center for Lung Research, Justus-Liebig-University Giessen, Giessen, Germany*
***4*** *Université Côte d'Azur, Laboratory of Clinical and Experimental Pathology and Hospital-Integrated Biobank (BB-0033-00025), CHU Nice, FHU OncoAge, IHU RespiERA, Nice, France*
***5*** *Département de Pneumologie, FHU-OncoAge, IHU RespiERA, CHU-Nice, France*
***6*** *Center for Interstitial and Rare Diseases and Cardiopulmonary Institute, Justus-Liebig-University Gießen, Giessen, Germany*
***7*** *European IPF Registry and Biobank*
***8*** *Laboratory BioSanté U1292, Univ. Grenoble Alpes, INSERM, CEA, 38000, Grenoble, France*

***** Contributed equally
# Correspondence to Bernard Mari, Institut de Pharmacologie Moléculaire et Cellulaire, CNRS-UMR-7275, Université Côte d'Azur, 660 route des Lucioles, F-06560. Email: mari@unice.fr

## ABSTRACT

*Introduction and main objectives*: Idiopathic pulmonary fibrosis (IPF) is a chronic, progressive and irreversible interstitial lung disease (ILD), that increases dramatically in incidence and prevalence with age. While successful alveolar regeneration after injury depends on pulmonary capillary endothelial cells (PCEC) reprogramming, the steps involving PCEC during lung injury and resolution as well as the influence of aging are unknown.

*Methods:* We used single-cell RNA-seq (scRNA-seq) and spatial transcriptomics to compare the transcriptome of bleomycin-induced fibrotic lungs of young (7 weeks) and aged (18 months) mice, at 3 time points corresponding to the peak of fibrosis (14 days), regeneration (28 days) and resolution (60 days).

*Results:* Among the 44541 sequenced and annotated cells, we confirmed the transcriptomic dynamics of several cell types including macrophages, in which conversion is conserved between young and aged mice. We also found that lung injury shifts the transcriptomic profiles of recently described PCEC cell types, with 4 prominent signatures. These signatures are characterized by the overexpression of *Lrg1* and are associated with pro-angiogenic signaling, potentially supported by adjacent cell types into the alveolar niche. These signatures were not equally maintained through the resolution process and between young and old animals. Moreover, part of this set of resolution-associated markers was also detected in pulmonary endothelial cells (ECs) from IPF samples. Finally, we found that aging also altered the transcriptome of general capillary cells (gCap) which display typical pro-fibrotic and pro-inflammatory features.

*Conclusions:* We provide a detailed characterization of the cellular dynamics associated with fibrosis development and resolution in young and aged lungs and propose that age-associated alterations in specific PCEC subpopulations may interfere with the process of lung progenitor differentiation contributing to the persistent fibrotic process typical of human pathology.

## INTRODUCTION

Gas exchanges between the external environment and the cardiovascular system take place in the lung alveoli through the thin membrane separating pneumocytes and the capillary plexus formed by pulmonary capillary endothelial cells (PCEC), supported by mesenchymal cells. This alveolar niche, whose homeostasis is constantly threatened by external aggressions, deploys high regeneration abilities through various mechanisms [1, 2]. Inadequate responses can lead to the development of chronic diseases such as idiopathic pulmonary fibrosis (IPF), an age-related pathology characterized by the accumulation of collagen-producing mesenchymal cells (myofibroblasts) resulting in the remodeling of the alveolar environment and accumulation of extracellular matrix (ECM), leading to progressive destruction of the parenchyma [3, 4]. IPF is the canonical progressive interstitial lung disease (ILD) associated with progressive decline in lung function and a median survival time of less than five years after diagnosis. Although two treatments are available to manage the disease (ie: nintedanib and perfenidone) and several new therapeutic options are under investigation, there is no curative treatment for IPF to date. Ultimately, some affected individuals will require a lung transplant [5]. In this context, there is an urgent need for a better understanding of the underlying cellular and molecular mechanisms responsible for IPF. The pathogenesis of IPF is complex and largely unknown. Current hypotheses suggest that microrepetitive injuries of unknown origin to pulmonary epithelial cells in the aging lung results in ineffective repair with excessive wound healing, chronic inflammation, apoptosis of epithelial and endothelial cells (EC), activation of fibrogenic effector cells, formation of myofibroblasts foci, and finally excessive deposition of ECM resulting in the destruction of the lung architecture and the loss of lung functions [6]. Mechanisms linking aging to the development of pulmonary fibrosis are not fully understood and involve numerous cell-intrinsic and cell-extrinsic alterations. Among them, it has been proposed that genetic and epigenetic changes, loss of proteostasis, cellular senescence, metabolic dysfunction as well as stem cell exhaustion may contribute to the initiation and progression of fibrosis [7-10].

Following lung injury, the restoration of parenchymal tissue integrity depends in particular on the proliferative capacities of PCEC [11]. Recent studies showed that, in physiological conditions, PCEC are functionally heterogeneous, with two distinct cell types conserved in multiple mammal species [12]. Aerocytes (aCap), are specialized in gas exchanges with type 1 pneumocytes, whereas general capillaries (gCap) act as progenitor-like cells able to self-renew and to differentiate into aCap to maintain the homeostasis of the microvascular endothelium. Multiple studies also report various EC subpopulations emerging after lung injury in mouse models [13-15] or in the context of IPF [16]. Nevertheless, the precise contribution of physiological cell types to those pathological subpopulations are not fully known. Moreover, as the regenerative functions of EC decline with aging [17, 18], the impact of aging on the dynamic of EC subpopulations associated with alveolar niche regeneration after injury-induced fibrosis remain largely unaddressed [19].

The murine single intratracheal bleomycin instillation model is considered as the best-characterized animal model available for the preclinical assessment of potential therapies for pulmonary fibrosis [20]. After the acute inflammatory phase has subsided, bleomycin-instilled mice display alveolar epithelial cell remodeling and fibrosis, but unlike patients with IPF, the fibrosis progressively resolves, allowing to study the cellular and molecular mechanism associated with alveolar repair and regeneration. Furthermore, studies assessing bleomycin in older mice revealed more pronounced fibrosis, with mechanisms more reminiscent of IPF [21-24]. It has been notably suggested that aged mice suffer from impaired resolution or regeneration after injury [25-28] indicating that age-associated processes contribute to the persistent fibrosis that is observed in IPF.

In this context, the aim of the present study was to compare the fate of different cell populations present in the lungs after bleomycin-induced injury in young and aged animals, from the fibrotic response peak (14 days) until partial (28 days) and complete (60 days) resolution. Our work presents a detailed picture of the cellular dynamics associated with a delayed fibrosis resolution in aged lungs and suggests that age-associated alterations in specific PCEC subpopulations may interfere with the process of lung progenitor differentiation contributing to the persistent fibrotic process typical of human pathology.

## RESULTS

### Aging is associated with a delay in the resolution of lung fibrosis

Lungs of young (7 weeks) and old (18 months) mice were collected 14, 28 or 60 days after bleomycin challenge (**Fig. 1A**). We first analyzed the potential differences occurring between young and aged mice, using global classical parameters. We noticed a shift of fibrosis resolution between young and aged mice, as visualized by total hydroxyproline assay (**Fig. 1B**), histological analyses (**Fig. 1C**) and Sirius red assay (**Supplemental fig. S1A**) with a peak of fibrosis at day 14 in young mice followed by a progressive reduction of fibrosis at D28 while a strong fibrotic pattern was still detected at D28 in old mice. In both young and old animals, fibrosis resolution was almost complete at D60, with only a few limited fibrotic areas.

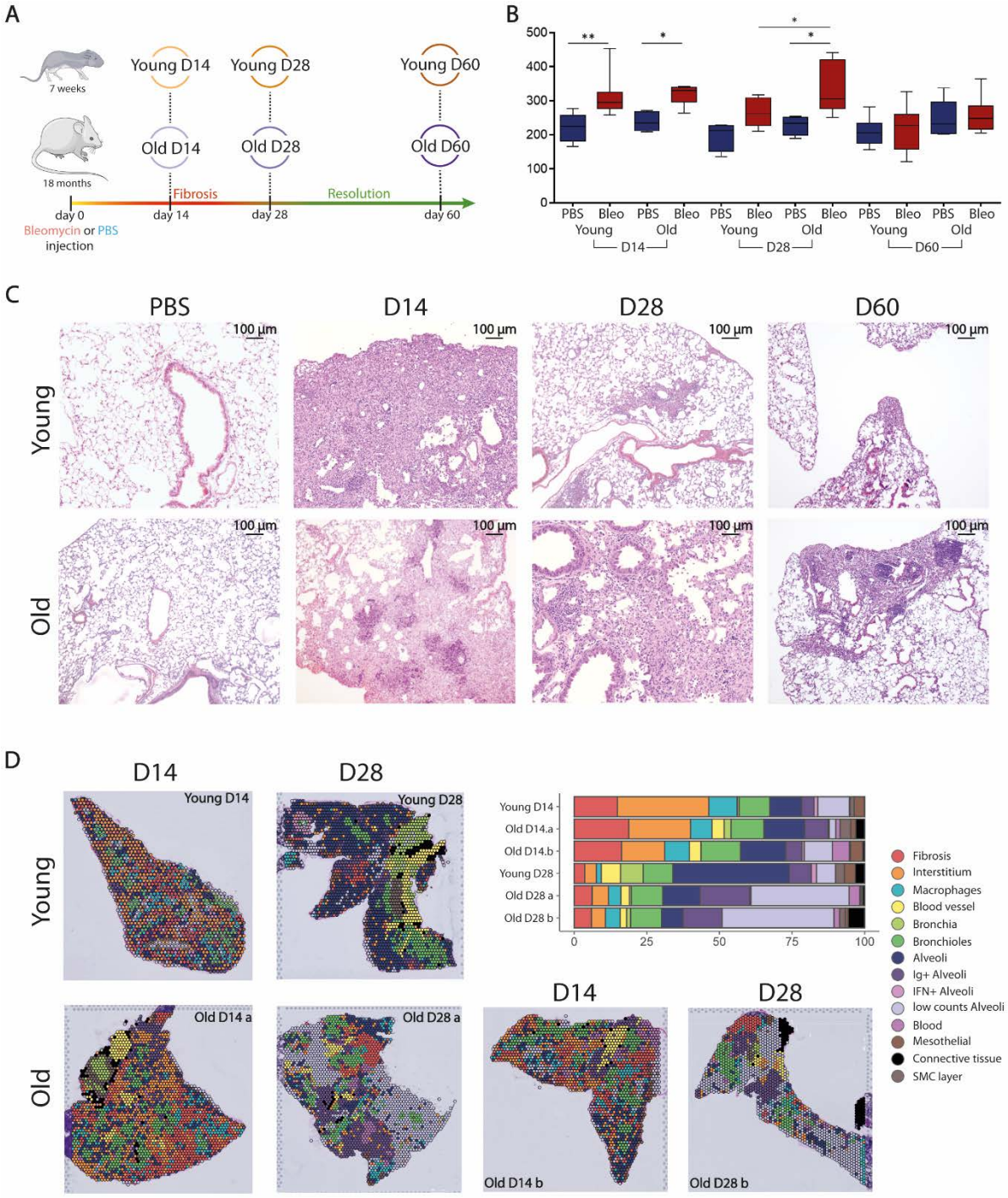


**Figure 1. Analyses of fibrotic parameters in bleomycin-injureg lungs from young and old mice.** **A,** Experimental design. Young (7 weeks) or old (18 months) mice were treated either with bleomycin

or PBS. Their lungs were collected at the bleomycin-induced fibrotic peak at day 14 and during lung regeneration (day 28) and fibrosis resolution (day 60). **B,** Hydroxyproline quantification on bleomycin or PBS treated young or old mice samples at indicated time points. (n=4-10/group). * P<0.05. ** P<0.01. P values were calculated by one-way ANOVA controlling the FDR using the Benjamini–Hochberg procedure. **C,** Histological sections of control and fibrotic lungs from young and old mice using HE at indicated time points. **D,** Spatial transcriptomics data from histological sections of lungs from young (n=1) and old (n=2) mice challenged with bleomycin and collected at fibrotic peak (day 14) and during regeneration (day 28). Spots are colored according to assigned tissue. The relative proportions of assigned tissues in each sample is displayed on top right part.

To better characterize this process, we performed a spatial transcriptomics experiment with the 10x Genomics Visium platform on lung sections from young or old mice taken 14 or 28 days after bleomycin instillation. For all spatial data samples, we performed an unsupervised assignation of each spot to a histological tissue/state (**Supplemental fig. S1B-D**) and compared the relative proportions of these histological types/states of tissue in each lung slice (**Fig. 1D**). Although the fibrotic areas were significantly reduced between days 14 and 28 for both ages, the alveolar areas of aged mouse lung sections from day 28 did not recover their functional integrity, unlike those of the young mouse section at the same time point. Indeed, about half of the spots from lung sections of aged mice 28 days post bleomycin injection were assigned to damaged alveolar regions, either characterized by low unique molecular identifiers (UMIs) content, aberrant expression of noisy genes (*Lars2, Gm42418, Malat1*) and epithelial markers (*Scbg1a1, Scgb3a1, Scgb3a2*) or by a signature of immunoglobulin superfamily genes and a decrease of physiological alveolar markers expressed by pneumocytes, fibroblasts and PCEC (**Fig. 1D, Supplemental fig. S1C-F and Supplemental table 1**). Overall, using various approaches, our data indicated that fibrosis resolution is delayed in lungs from aged mice.

**Time-resolved scRNA-seq captures cellular heterogeneity of bleomycin-injured lungs from young and aged mice.**

To better investigate the mechanisms of lung regeneration and the potential influence of ageing on resolution dynamics, we reproduced the same experiment and performed scRNA-seq on whole lungs of young (7 weeks) and aged (18 months) mice (n=3) collected 14, 28 or 60 days after bleomycin challenge ($2U.kg^{-1}$) or PBS (**Fig. 2A**). The conditions from each time point were multiplexed using cell hashing [29] to mitigate batch effects. The count matrices from the 36 sequenced samples were integrated to obtain a single dataset of 44,541 cells. Based on their transcriptomic profile, the cells were clustered and manually annotated based on the expression of specific marker genes (**Fig. 2B, Supplementary table 2**). We identified 41 populations recapitulating the cellular heterogeneity of the mouse lung, of which 29 were immune cells from lymphoid or myeloid lineage, such as alveolar macrophages (AMs). We also detected mesenchymal cells, including fibroblasts, pericytes, mesothelial cells as well as epithelial populations such as type 1 alveolar cells (AT1), type 2 alveolar cells (AT2) and multiciliated cells. We finally identified 6 endothelial populations: proliferating EC (Prolif. EC), gCap, aCap, pulmonary-venous EC (PV EC), arterial EC and lymphatic EC. As expected, we observed a shift in several populations following bleomycin injury (**Fig. 2C and Supplemental table 3**). This was particularly the case for macrophages, as previously described [30-32], with a rapid influx of recruited monocyte-derived macrophages (Mo-AMs) AM3 populations along with a drop of the tissue-resident (TR-AMs) AM1. Other cell types affected upon bleomycin injury also include fibroblasts (**Fig. 2C**). However, the low number of fibroblasts captured in our dataset did not allow a precise description of the different subpopulations, as already shown by different studies [33-36]. Epithelial cells, including notably alveolar AT1 and AT2 cells were also excluded from a specific analysis due to their reduced cell number in our dataset. Finally, bleomycin injury induced major alterations in pulmonary EC types, especially gCap, PV EC and aCap (**Fig. 2C**), suggesting underlying cellular heterogeneity in bleomycin-treated mice.

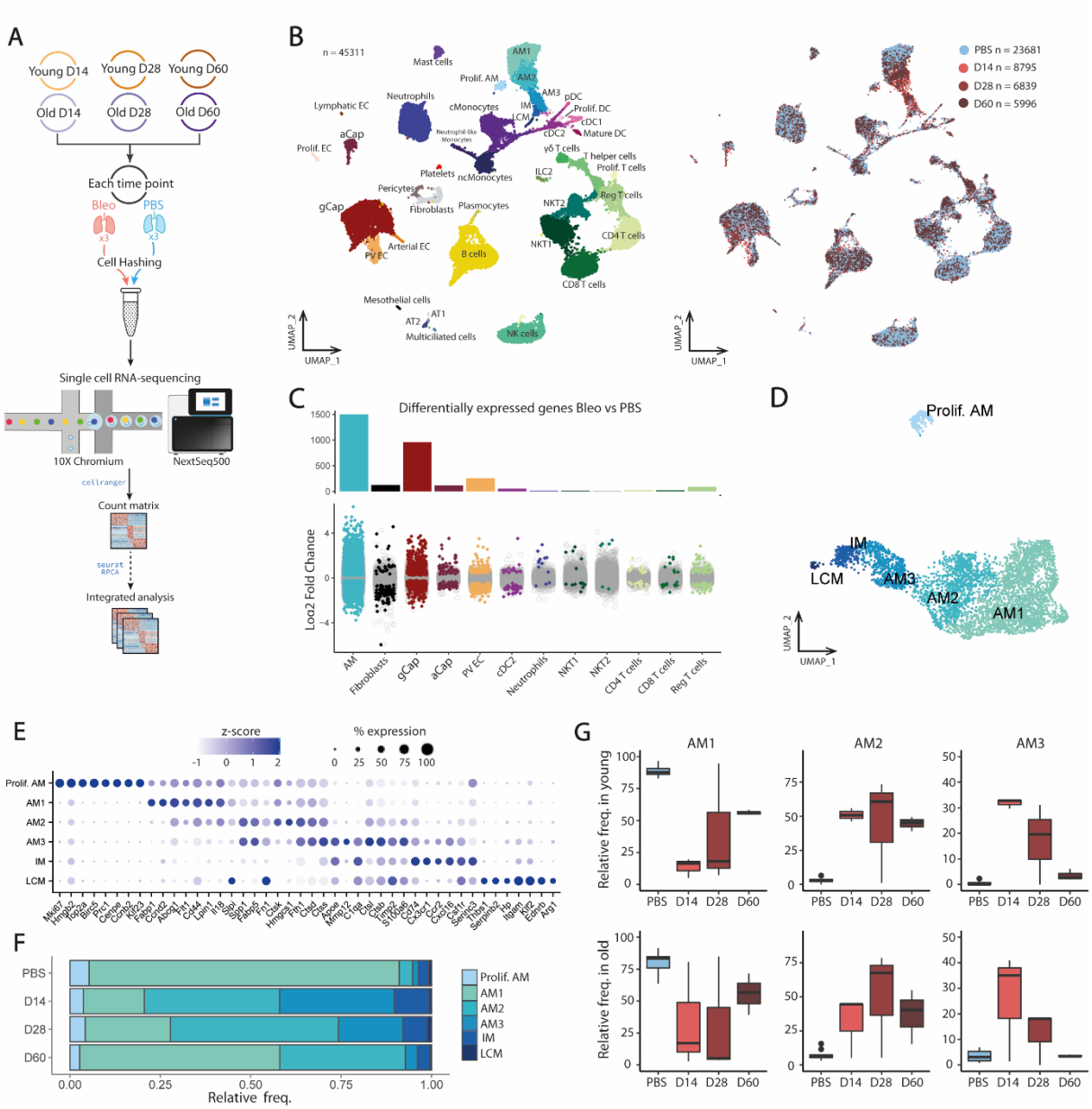


**Figure 2. Time-resolved scRNA-seq captures pulmonary cell populations heterogeneity in bleomycin-injured lungs from young and old mice.** (A) scRNA-seq experimental design. (**B**) UMAP of the integrated dataset of the 45311 sequenced cells. Cells are colored according to the annotated clusters (left) or time point (right). Prolif. AM = proliferating macrophages; AM = alveolar macrophages; IM = interstitial macrophages; LCM = large-cavity macrophages; Prolif. DC = proliferating dendritic cells; cDC = conventional dendritic cell; Mature DC = mature dendritic cells; pDC = plasmacytoid dendritic cells; cMonocytes/ncMonocytes = conventional/non-conventional monocytes; Prolif. T cells = proliferating T cells; Reg T cells = regulatory T cells; ILC2 = type 2 innate lymphoid cells; NKT = natural killer T cells; NK cells = natural killer; AT1/2 = Alveolar Type 1/2 cells. (**C**) Differentially expressed genes (DEGs) between Bleomycin and PBS treated cells for indicated populations. The number of DEGs is limited to 1500 for the bar plot. (**D**) UMAP of macrophages AM = Alveolar Macrophages, IM = Interstitial Macrophages, LCM = Large Cavity Macrophages. (**E**) Markers of macrophages subpopulations. (**F**) Relative proportions of macrophages subpopulations in indicated time points. (**G**) Relative proportions of macrophages subpopulations between young and old across time points.

## The dynamics of macrophage sub-populations associated with lung fibrosis and resolution is similar in young and aged mice.

Given the importance of specific macrophage subpopulations in lung fibrogenesis [37], we then wondered whether differences in macrophage subsets dynamics may also reflect this aging-dependent delay of resolution. We identified six subsets of macrophages with specific gene

signatures, including proliferating macrophages (Prolif. AM), 3 subpopulations of alveolar macrophages (AM1, AM2, AM3), interstitial macrophages (IM) and large-cavity macrophages (LCM) (**Fig. 2D-E and Supplemental table 2**). We evaluated the impact of age on the frequency of each subpopulation relatively to the total number of cells analyzed in each mouse treated with PBS or BLM (**Fig. 2D-E and Supplemental fig. S2A-B**). A very similar profile was observed for all populations in both the young and old animals. In particular, we observed a rapid drop of the Fabp1+ AM1 upon BLM administration along with an influx of Spp1+ AM3 at the peak of fibrosis, likely corresponding to Mo-AMs. During the resolution phase, the proportion of Mo-AMs (AM3) progressively decreased to less than 5% at D60. Interestingly, AM2, an intermediate population sharing both AM1 and AM3 markers also appeared during the fibrotic phase but then maintained stable until day 60. Overall, bleomycin treatment induced a very similar dynamics of macrophage subsets in young and old animals from the peak of fibrosis to complete resolution indicating that none of these specific subpopulations appear to be associated with the delayed resolution in aged animals.

**Lung injury shifts PCEC towards Lrg1+ subpopulations**

The subclustering of PCEC and macrovascular subsets revealed the emergence of four new subpopulations in bleomycin-injured lungs from both young and aged mice (**Fig. 3A-B**). Among these subclusters, two new subpopulations of gCap and aCap cells emerged in fibrotic lungs with recognizable signatures particularly characterized by the overexpression of Leucine-rich α-2 glycoprotein 1 (*Lrg1*) and mostly found at day 14 and day 28 following bleomycin treatment (**Fig. 3C-D**). The Lrg1+ gCap cells subpopulation expressed specific gCap markers such as *Aplnr* but also exhibited high expression levels of *Lrg1* together with a signature including *Ackr3, Tmem252, Cmah, Ankrd37, Ntrk2* or *Plac8* (**Fig. 3B, Supplemental table 2**). In a similar way, we identified Lrg1+ aCap, expressing specific aCap markers such as *Ednrb*, but highly expressing *Lrg1* in the pathological context as well as *Tnrfrsl11b, Serpine1, Fgfr1, Ankrd37* or *Dnah11* (**Fig. 3B, Supplemental table 2**). The third population matched a cluster of proliferating PCEC (Prolif. EC), expressing both cell-cycle genes (*Ube2c, Hmmr, Pbk, Gas2l3, Aurkb*) and capillary markers, which was only found at day 14 and to a lesser extent at day 28 following bleomycin treatment (**Fig. 3B-C**). Finally, a fourth population corresponded to Col15a1-positive systemic venous vessels (SV EC), localized specifically to systemically supplied vessels of the bronchial vascular plexus and of the visceral pleura under physiological conditions [38] and recently found widespread in fibrotic areas of IPF patients [16]. This homologous murine population shared, to some extent, the expression of others markers found in human cells, such as *Hspg2, Nrp2, Gja1, Vwa1, Lamb1, Spry1, Filip1, Ndrg1, Nr5a2, Galnt15* and *Meox1* (**Fig. 3B-C, Supplemental table 2 and Supplemental fig. S2B**). Others markers of SV EC were restricted to the murine model, such as *Rgcc, Rflnb, Trp53i11, Arhgap18* or *Fscn1*. We noted that this population described as being of macrovascular origin shares some markers with gCap, such as *Aplnr, Sox11* or *Sema3g* (**Fig. 3B-C)**. We hence considered them as another PCEC subpopulation for the rest of the study. The two others macrovascular cell types are Col15a1-negative pulmonary-venous (PV EC) and arterial endothelial cells, expressing canonical markers *Slc6a2* and *Atp13a3* respectively [38] (**Fig. 3B-C and Supplemental table 2)**. The proportions of these latter cell types remained constant before and after injury (**Fig. 3D)**.

*Lrg1* is a gene coding for a pro-inflammatory glycoprotein capable of modulating TGF-β signaling, which can notably promote angiogenesis [39]. In physiological condition, *Lrg1* expression is restricted to PV EC, Neutrophils, LCM, and to a lesser extent to AT2, gCap and Lymphatic EC **(supplemental fig. S2D).** At the peak of fibrosis, *Lrg1* expression was dramatically increased in all endothelial subpopulations as well as in alveolar macrophages subsets **(Supplemental fig. S2E)**. We confirmed this increase of Lrg1 in bleomycin-treated lungs by *in situ* hybridization **(Supplemental fig. S2F)**. *Lrg1* expression decreased to basal levels during the resolution phase, except in persistent SV EC and alveolar macrophages in which it remained highly expressed even 60 days BLM post-instillation. The kinetics of *Lrg1* expression in old versus young mice treated with BLM was similar in most subpopulations,

apart for gCap, aCap and Arterial EC, for which *Lrg1* expression was time-shifted at day 28 **(Supplemental fig. S2G).**

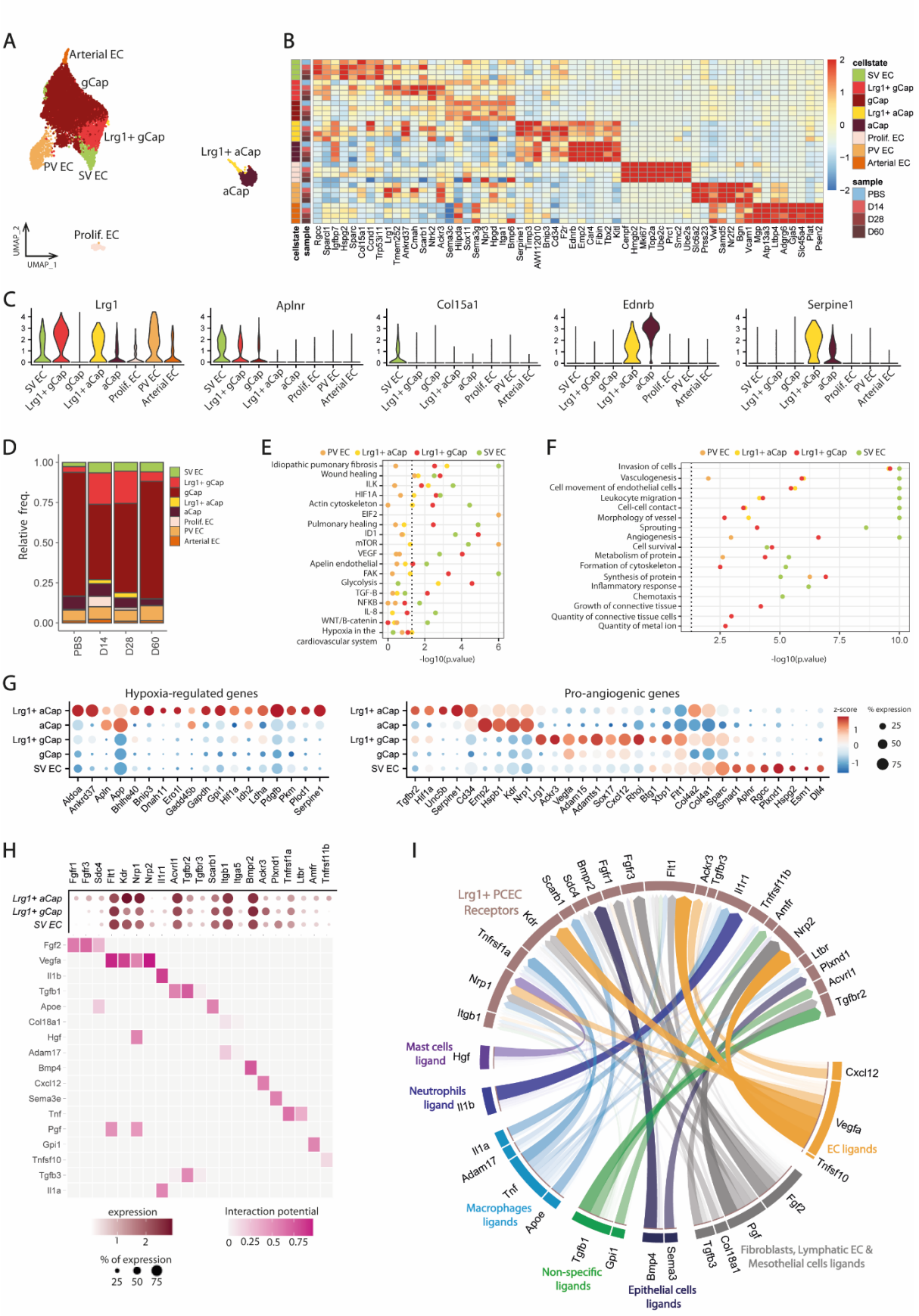

**Figure 3. Lung injury shift pulmonary endothelial cells towards Lrg1+ subpopulations associated with lung alveolar niche regeneration. (A**) UMAP of pulmonary EC subpopulations. gCap = general capillaries cells, aCap = aerocytes, SV EC = systemic venous endothelial cells, PV EC = pulmonary-venous endothelial cells. (**B**) Heatmap of top EC subpopulations markers. All cells from young and aged mice with all treatments are pooled. Expression is indicated as a z-score. (**C**) Normalized expression of *Col15a1, Lrg1, Aplnr, Serpine1* and *Ednrb*. (**D**) Relative proportions of PEC subpopulations across time points. (**E**) Selection of top activated canonical pathways in Lrg1+ PCEC subpopulations. (**F)** Selection of top activated functions in Lrg1+ PCEC subpopulations. (**G**) Level and percentage of expression of hypoxia-regulated (left) and pro-angiogenic (right) genes in Lrg1+ PCEC subpopulations. (**H**) Level and percentage of expression of *bona fide* receptors in Lrg1+ PCEC subpopulations (top); interaction potential with the prioritized ligands (bottom) as predicted by NicheNet analysis. (**I**) Circos plot of ligands-receptors interactions predicted by NicheNet analysis. Ligands are colored according to their specific expression.

Finally, we validated the overexpression of Lrg1 in gCap and aCap using an independent scRNA-seq dataset [40] in which lungs of adult mice treated with bleomycin were collected at a shorter time interval **(Supplemental fig. S2H).** These data showed an increased *Lrg1* expression level in both aCap and gCap starting 7 days following bleomycin challenge, corresponding to the initiation of the fibrotic phase. These findings demonstrate that bleomycin injury induces pulmonary EC remodeling and the emergence of distinct capillary cell states according to *Lrg1* expression status.

**Lrg1+ PCEC signaling is associated with vascular remodeling and alveolar regeneration.**

We performed Ingenuity Pathway Analysis™ on SV EC, Lrg1+ gCap and Lrg1+ aCap markers, and then on PV EC. The IPF, mTOR signaling, TGF-β signaling, integrin-linked kinase signaling and wound healing pathways were significantly activated in the 3 PCEC subpopulations (**Fig. 3E)**. SV EC and Lrg1+ gCap also shared an upregulation for ID1, EIF2, HIF1A, VEGF, FAK, WNT/β-catenin and actin cytoskeleton signaling, whereas IL-8 signaling was found restricted to SV EC. Both Lrg1+ aCap and Lrg1+ gCap markers were associated with glycolysis and hypoxia in the cardiovascular system. We observed that most of those pathways were not activated in PV EC. In terms of enriched functions, SV EC, Lrg1+ gCap and Lrg1+ aCap signatures reflected the activation of angiogenesis or vasculogenesis, endothelial cell migration and proliferation, which are not found or to a lesser extent in PV EC (**Fig. 3F)**. Based on these results, we further examined the expression profiles of hypoxia-regulated genes and we noted that Lrg1+ aCap was the PCEC subpopulation showing the strongest signature with high expression levels of genes such as *Ankrd37, Bhlhe40, Bnip3, Dnah11, Plod1* or *Serpine1* (**Fig. 3G)**. Similarly, we looked at the expression of Lrg1+ PCEC markers associated with angiogenesis. Overall, their expression was shared by all 3 Lrg1+ PCEC subpopulations, with some expression specificity for several genes, such as tip cells markers *Esm1* and *Dll4* restricted to SV EC. The signature was composed of genes coding for extracellular matrix (ECM)-associated proteins (*Sparc, Col4a1, Col4a2, Adam15, Adamts1, Hspg2*), transcription factors/regulators (*Smad1, Xbp1, Sox17, Hif1a*), but also for cytokines/growth factors (*Cxcl12, Vegfa, Btg1*) and receptors (*Aplnr, Ackr3, Tgfbr2, Nrp1, Kdr, Flt1, Plxnd1*), suggesting a central role for Lrg1+ PCEC in endothelial regeneration processes via intense signaling within the alveolar niche (**Fig. 3G)**.

To follow up this hypothesis, we used NicheNet [41] to infer ligand-receptor interactions potentially associated with the expression of genes related to the pro-angiogenic signature of Lrg1+ PCEC. According to the NicheNet model, we selected the top ligands with the highest probability to induce these pro-angiogenic signatures in each Lrg1+ PCEC subpopulation. Most of the selected ligands were commonly prioritized in the 3 subpopulations and were known pro-angiogenic factors, such as *Fgf2*, *Vegfa*, *Il1b*, *Tgfb1*, *Apoe*, *Bmp4*, *Adam17* or *Cxcl12* **(Supplemental fig. S3A).** *Tnfsf10* and *Tgfb3* were only prioritized in Lrg1+ aCap, and Il1a was specifically prioritized in Lrg1+ gCap. We next looked at the expression of the selected ligands as well as the downstream genes most likely to be regulated by these ligands in the

different lung cell populations **(Supplemental fig. S3A)**. Notably, *Vegfa* and *Cxcl12* ligands were among the top predicted ligands as well as the top predicted downstream-regulated genes, suggesting autocrine signaling within Lrg1+ PCEC. We finally checked the expression of genes encoding *bona fide* receptors of the selected ligands in the 3 Lrg1+ PCEC subpopulations (**Fig. 3H)**. Overall, their transcripts were equivalently detected in the 3 Lrg1+ EC subpopulations, with the exception of Fgf2 receptors Fgfr1 and Fgfr3 which are more specific to the Lrg1+ aCap. We have summarized these interactions inferences in a circos plot, linking the selected ligands grouped by expression in specific cell populations to their top receptors expressed in Lrg1+ PCEC subpopulations (**Fig. 3I)**. We represented potential paracrine and autocrine signaling involving ligands expressed by mast cells (*Hgf*), neutrophils (*Il1b*), macrophages (*Il1a*, *Adam17*, *Tnf* and *Apoe*) as well as ligands expressed in multiple cell types such as *Tgfb1* and *Gpl1*. We also found potential interactions between ligands of neighboring cell types within the alveolar niche and Lrg1+ PCEC receptors, such as the *Bmp4* / *Bmpr2* pair involving alveolar epithelial cells and the *Tgfb3* / *Tgfbr* pair with mesenchymal cells. The specific expression of *Fgfr1* and *Fgfr3* in Lrg1+ aCap as well as the upregulation of *Plxnd1* in SV EC suggested that communication with *Fgf2*-expressing fibroblast and *Sema3e*-expressing alveolar epithelial cells could be more restricted to Lrg1+ aCap and SV EC, respectively. Based on the hypothesis that a receptor differentially expressed between physiological and fibrotic conditions likely indicates a modulation of the associated signaling pathway, we then compared receptor expression levels between gCap from bleomycin- versus PBS-treated mice. We observed that Ackr3, Il1r1, Itgb1, Nrp2, Scarb1, Sdc4 and Tgfbr2 were all upregulated while Bmpr2 and Tgfbr3 were downregulated in bleomycin-treated compared to control gCap **(Supplemental fig. S3B)**. These observations appear consistent in the context of capillary endothelial remodeling. For example, the autocrine signaling pathway involving *Cxcl12* and *Ackr3* in PCEC has been shown to drive alveolar epithelial cells expansion and neo-alveolarization by releasing Mmp14 following lung injury [42]. Our analysis indeed validated the upregulation of Mmp14 in bleomycin-treated gCap at the single cell transcriptomic level **(Supplemental fig. S3C)**. Finally, we also checked if others genes driving key signal transduction proteins in EC, such as ALK1, ALK5, ENG, ID1 and SMADs, were differentially expressed between both conditions in gCap **(Supplemental fig. S3D)**. In particular, we found that *Smad6* was significantly downregulated in bleomycin-treated gCap. Coupled with the repression of *Bmpr2* and a similar trend for other BMP9 signaling pathway-associated genes (*Acvrl1*, *Eng*, and *Id1*), we hypothesized that this pathway responsible for endothelial quiescence may be inhibited in gCap following lung injury to promote angiogenesis [43]. Taken together, these results converge towards pro-angiogenic signaling in Lrg1+ PCECs which, by releasing angiocrine factors, could thus contribute to the regeneration of the pulmonary alveolar niche.

**Lrg1+ PCEC dynamics are delayed in fibrotic aged mouse lungs.**

In order to compare the dynamics of pulmonary ECs after injury and during resolution between young and old mice, we first looked at the evolution of their relative frequencies at different times following bleomycin treatment (**Fig. 4A**). The proportion of SV EC, which were weakly detected in the control lungs, increased after bleomycin instillation and progressed during the resolution phase, suggesting that SV EC recruitment is sustained over time independently of aging. Conversely, both Lrg1+ gCap and Lrg1+ aCap cells displayed a different kinetic profile following bleomycin treatment in young and aged mice. While these 2 populations peaked at day 14 in young mice lungs, they appeared progressively in the lungs of aged mice, peaking at day 28 and tending to disappear after 60 days. The proliferating PCEC dynamic was similar in young and old mice, with an increase from 0 to 10% at day 14 followed by a quick disappearance during resolution. PV EC, which appeared to be more abundant in old animals in physiological conditions, were only increased in young mice after lung injury and progressed during the resolution phase. Consistently between young and old, gCap fully recovered during the resolution phase after a sharp drop at the peak of fibrosis, whereas the pool of aCap tended to decrease over time after bleomycin challenge. These observations suggest that the

transcriptional remodeling of gCap into Lrg1+ transitory subpopulations may affect their abilities to differentiate and replenish the pool of functional aCap.

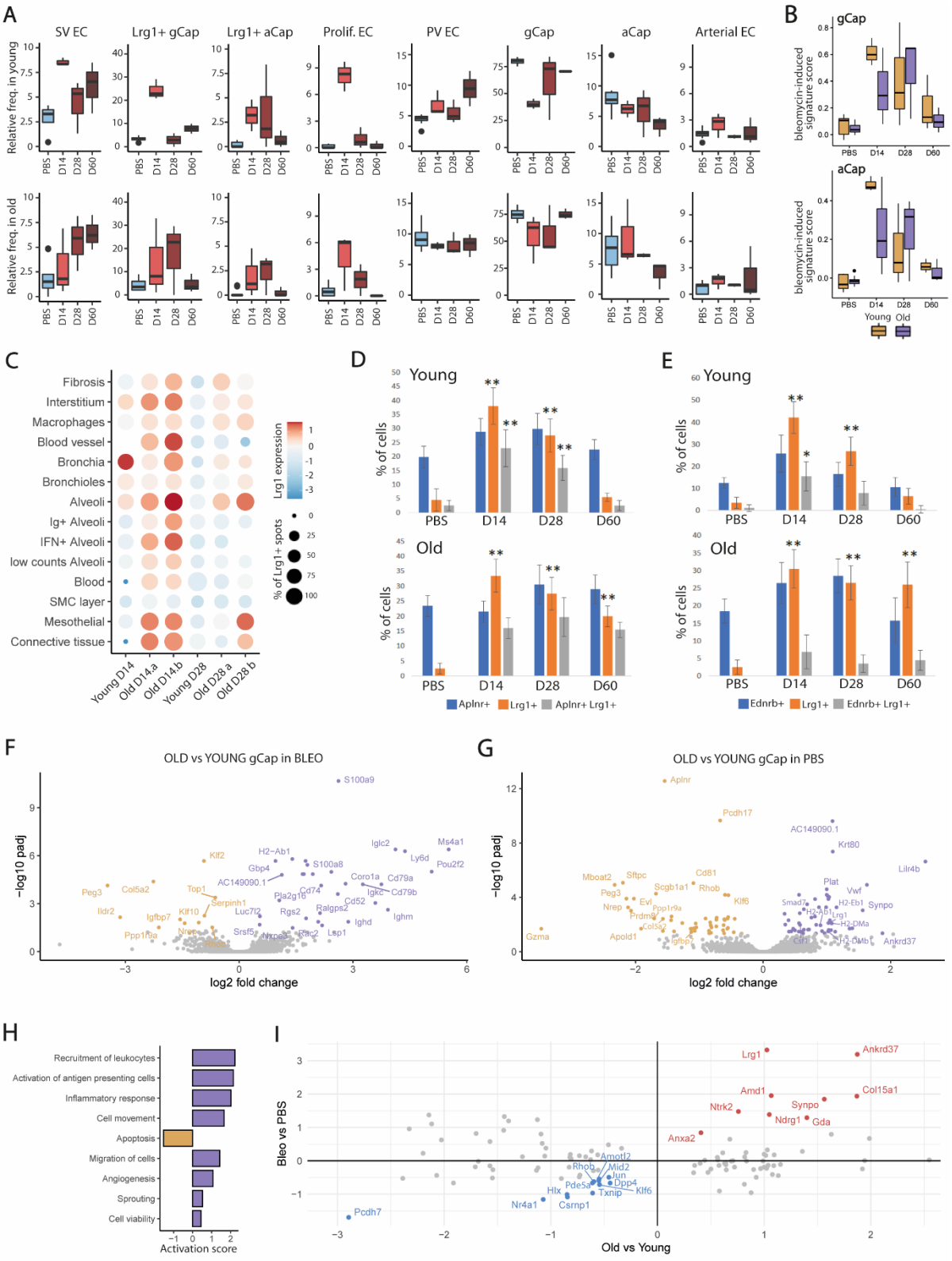


**Figure 4. Lrg1+ PCEC dynamics are delayed in old mice, which display a pro-inflammatory phenotype in pathological condition and a pre-fibrotic phenotype in physiological condition.** (**A)** Pulmonary endothelial subpopulations relative frequencies in young and old mice across time points. (**B)** Bleomycin-induced signature score (see material and methods section) in gCap (top) and aCap (bottom) in young and old mice across time points. (**C)** Spatial transcriptomic expression of Lrg1 in

annotated spots from each sample. (**D-E**) In situ hybridization of Lrg1 with gCap marker Aplnr (**D**) or aCap marker Ednrb (**E**) at indicated time points in young (top) and old (bottom) mice. (n=3). Quantification was performed in three different fields for each mouse. * P<0.05, ** P<0.01. P values were calculated by a two-tailed Mann–Whitney test (**F)** Differentially expressed genes (DEGs) between old and young gCap in fibrotic condition. (**G)** DEGs between old and young gCap in physiological condition. (**H)** Functions enrichment analysis on DEGs between young and old physiological gCap. (**I**) Comparison between the ageing-associated DEGs in physiological condition and the bleomycin induced signature in gCap.

We also compared the bleomycin-induced transcriptomic signatures in aCap and gCap cells from young and aged mice lungs at each time point following bleomycin instillation. The expression of upregulated genes in the fibrotic phase (day 14 and day 28) compared to control condition were used to compute a score in each cell (**Fig. 4B and Supplemental fig. S4A-B**). While the bleomycin-induced signature score peaked at day 14 in aCap and gCap from young mice, it also shifted towards day 28 in aged animals. We found a similar profile for the bleomycin-induced signature score in PV EC (**Supplemental fig. S4C**).
We next reanalyzed our spatial transcriptomic dataset. The resolution of the Visium$^{TM}$ spatial transcriptomic protocol did not allow us to identify specific spots corresponding to physiological or pathological PCEC, but we were able to detect specific markers in several areas, notably in fibrotic regions, interstitium and alveoli (**Supplemental fig. S4D**). In particular, the expression of *Lrg1*, which was high and diffuse at day 14 in most annotated areas, persisted at day 28 in several areas of the sections from aged mice including alveoli and fibrotic regions, whereas it returned to low expression levels in the corresponding sections of young mice (**Fig. 4C**).
We finally performed *in situ* hybridization assay of *Lrg1* with either the gCap marker *Aplnr* or the aCap marker *Ednrb* on lung sections of young and aged mice treated with PBS or Bleomycin at the same 3 time points **(Fig. 4D-E and Supplemental fig. S5**). We confirmed that in young mice, *Lrg1* was highly upregulated at day 14 following bleomycin treatment and progressively decreased until it returned to its basal level at day 60, whereas its overexpression was maintained at day 28 and day 60 in old mice. Similarly, we observed the same evolution pattern with Lrg1+ Aplnr+ cells and Lrg1+ Ednrb+ cells, corresponding to Lrg1+ gCap and Lrg1+ aCap, respectively.
Taken together, our results showed that the dynamics of Lrg1+ PCEC cells are delayed in lungs from aged mice compared to young, with the persistence of both Lrg1+ gCap and Lrg1+ aCap cells in specific areas, paralleling the kinetic profile observed for the resolution of lung fibrosis between young and aged mice.

**Aged mouse lung gCap cells exhibit pro-inflammatory and pre-fibrotic phenotype**
We next evaluated the impact of ageing on the transcriptomic signature of PCEC. We focused on the gCap population that is already present in physiological conditions and functions as progenitor cell in capillary homeostasis and repair. We performed differential expression analyses between old and young gCap in fibrotic (Bleo day 14 and Bleo day 28) and control “physiological” conditions (PBS). In fibrotic conditions, we observed an enriched pro-inflammatory signature in old gCap, characterized by the overexpression of *S100a8, S100a9* and genes encoding for proteins of the immunoglobin super family, such as antigen receptors (*Igcl2, Igkc, Ighm, Ighd, CD79a, CD79b*) which correlates with the upregulation of the immunoglobulin gene regulator *Pou2f2*, antigen presenting molecules (MHC-II (*H2-Ab1, H2-DMb1, H2-Eb1, H2-DMa, H2-Aa*)) and other surface markers such as *Ms4a1, Ly6d, Cd74* or *Cd52* **(Fig. 4F and Supplemental table 4**). Conversely, we found in young gCap an enrichment of transcription factors associated with vascular homeostasis and repair such as *Klf2, Klf10 and Peg3* [44-47]. In PBS-treated mice, comparison between old and young gCap revealed even more gene modulations, which were associated to multiple functions **(Fig. 4G-H and Supplemental table 5**). Among the top upregulated functions in old gCap, we found the inflammatory response as in the fibrotic condition, but only supported by antigen presenting molecules (MHC-II (*H2-Ab1, H2-DMb1, H2-DMa, H2-Eb1, H2-Aa)*). Like the signature of young fibrotic gCap, *Peg3, Ppp1r9a, Col5a2, Igfbp7, Nrep,* and *Rhob* were found enriched in young physiological gCap compared to old ones. In the PBS condition only, we also observed that

old gCap overexpressed Csf1*, Lilr4b, Plat*, *Smad7* and *Vwf*, which is normally restricted to macrovascular EC **(Fig. 2E),** while showing a decrease of *Aplnr* compared to young gCap, suggesting a potential change in their intrinsic functions. In addition, we found significant enrichment for genes associated with angiogenesis, migration and sprouting, such as for the bleomycin-induced signature in gCap. To go further, we directly compared the list of differentially expressed genes (DEGs) between old and young Cap in physiological condition to the list of DEGs between bleomycin-treated and PBS-treated gCap **(Fig. 4I)**. We observed an intersection of 9 genes commonly upregulated in old physiological gCap and in gCap following bleomycin challenge, as well as 12 genes down-regulated in gCap from both old control mice and bleomycin-treated mice. Among the 9 genes upregulated in both the ageing and lung injury signatures, we found the top Lrg1+ PCEC markers *Lrg1, Col15a1, Nrtk2, Ndrg1* and *Ankrd37.* These findings indicate that old gCap in physiological condition already express a pro-inflammatory and pro-fibrotic signature that is exacerbated after lung injury. In addition, they present a transcriptomic profile more similar to macrovascular endothelial cells and to bleomycin-induced Lrg1+ PCEC subpopulations.

**Bleomycin-induced endothelial remodeling echo pathological signatures found in human IPF**

In order to establish a link between the endothelial remodeling induced after lung injury in the mouse model and human IPF, we re-analyzed the pulmonary endothelial subset from a public scRNA-seq dataset obtained from lungs of transplanted patients with IPF or from healthy donors [48] (**Fig. 5A)**. As already described [16], the repartition of pulmonary EC subpopulations is shifted in IPF samples, with a clear increase of the COL15A1-positive SV EC proportion at the expense of others cell types (**Fig. 5B-C)**. In agreement with these data, we confirmed the co-expression of COL15A1 in a fraction of CD31+ endothelial cells in fibrotic areas of lung IPF sections (**Fig.5D and Supplemental fig. S6A**) while COL15A1+ EC were also found localized to systemically supplied vessels of the bronchial vascular plexus in both normal and IPF sections, as previously described [38]. We observed a low expression of *LRG1* in SV EC from IPF samples. We did not detect *LRG1* either in gCap or aCap from IPF samples, but decreased *EDNRB* and increased *SERPINE1* were observed in aCap, as in aCap from bleomycin-treated mice **(Fig. 5C)**. We then systematically compared the mouse fibrotic signature induced by bleomycin with the IPF signature in SV EC, PV EC, gCap, and aCap (**Fig. 5E-F and Supplementary table 6**). We found that the most conserved pathological signature in both models is for SV EC, with a common modulation of 218 genes. Among the conserved upregulated genes, we detected most of the pro-angiogenic signature enriched in mouse Lrg1+ PCEC: *COL4A1, COL4A2, SPARC, CD34, KDR, CXCL12, SOX17, RHOJ, RGCC, HIF1A, SMAD1, PDGFB, FLT4, ENPP2* and *APLNR*. Moreover, we observed a conserved upregulation of other signaling-associated genes such as *VWA1, INHBB, TNFRSF10B, PDGFB*, *SPRY1* or *APLN,* of other transcription factors like *NREP, EBF1, PRDM1* or *SOX4* and other ECM-associated genes like *COL15A1, LAMC1, LAMA4,* and *LAMB1.* This conserved signature also contains *IGFBP7* and *PDLIM1*, which are also conserved in PV EC and gCap. *PDLIM1*, which is also conserved in aCap, is a known inhibitor of NFKB-signaling [49] (as well as *RASSF2*, upregulated in SV EC of both models). With regard to conserved downregulated genes, we observed a common inhibition of transcription factors such as *CEBPD, GATA2, GATA6, HES1, FOXF1, KLF2, KLF4*, or *KLF9*; and signaling-associated genes such as *LTBP1, FGFR3, TGFB2, SRGN, VEGFC, VWF, THBD, SMAD7, TEK, EMP3*, or *DUSP1*. As observed in Lrg1+ PCEC, BMP9 signaling genes *BMPR2, ACVRL1, ID1* and *SMAD6* are repressed. These findings show that the pulmonary endothelial remodeling observed after bleomycin-induced lung injury in mice mimics the recruitment of SV EC occurring in IPF, whose transcriptomics profiles are highly conserved between the two models. These profiles share common regulation features with Lrg1+ gCap and gCap, suggesting a dynamic process linking those subpopulations.

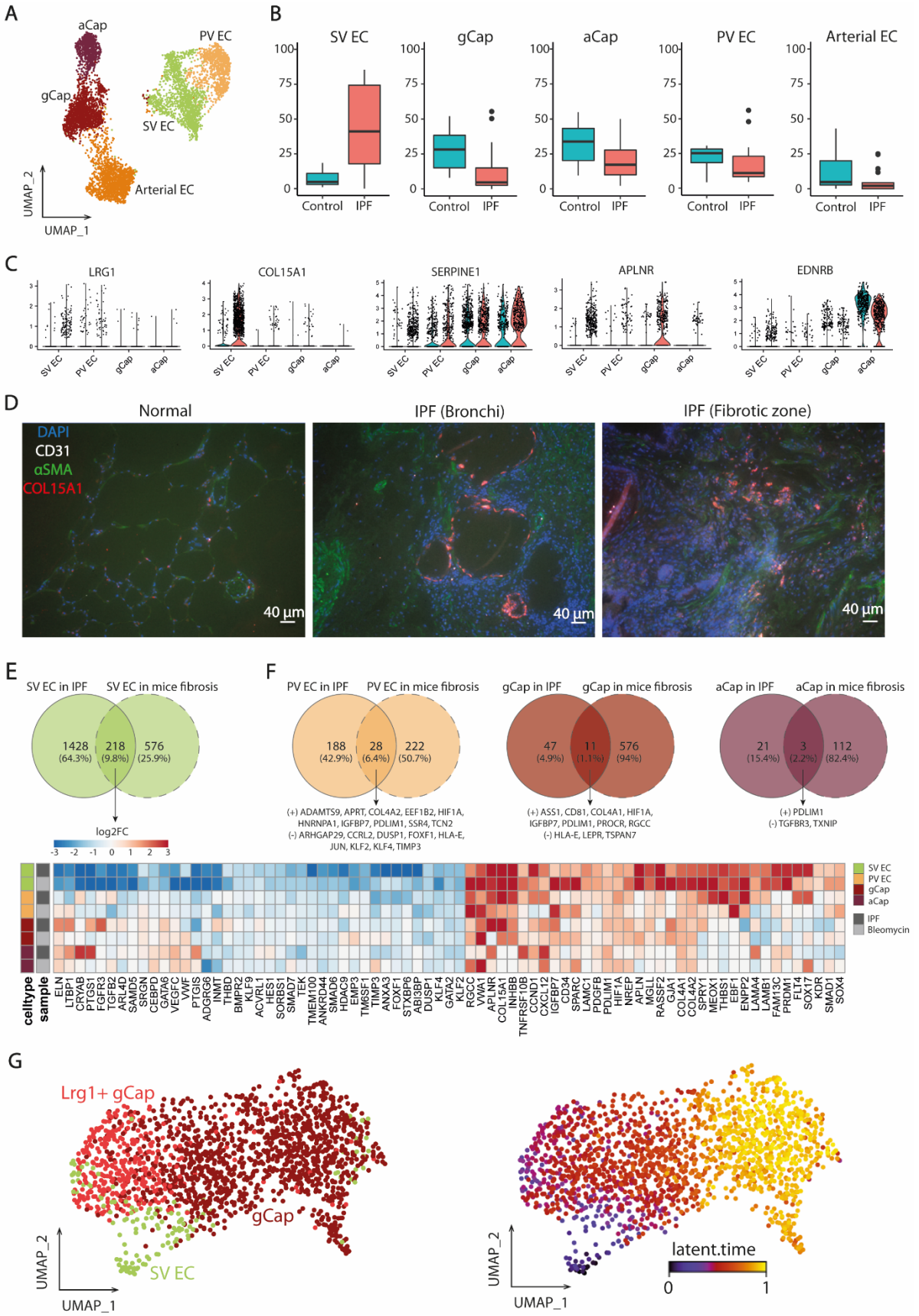


**Figure 5. Relevance of mice pulmonary EC pathological signatures in human IPF.** (**A)** UMAP of EC subpopulations in Habermann et al. dataset. (**B)** Relative proportion of EC subpopulations in Habermann et al. dataset. (**C)** Normalized expression of LRG1, COL15A1, SERPINE1, APLNR and EDNRB in EC subpopulations from control (blue) and IPF (light red) samples from Habermann et al.

dataset. (**D)** Expression of COL15A1 in lung sections from normal or IPF (bronchi and fibrotic areas) tissues by Immunofluorescence. Representative immunofluorescent images of COL15A1 or LRG1 (in red) with the pan EC marker CD31 (white) and αSMA (green). Nuclei are counterstained with DAPI (4′,6-diamidino-2-phenylindole). **(E)** Comparison of human and mouse fibrosis signatures in SV EC. Log2FC of similarly modulated genes are displayed in the heatmap. (**F)** Comparison of human and mouse fibrosis signatures in PV EC, gCap and aCap. (**G)** UMAP computed on Young D14 mice spliced RNA data (3 Bleomycin and 3 PBS-treated mice), with cells colored by PCEC subpopulation (left) and RNA velocity latent time (right).

To model a potential trajectory in an unbiased way, we used the generalized RNA velocity approach [50], leveraging on the splicing dynamics estimated in young bleomycin and PBS-treated mice samples at day 14. Latent time ordering indicated that SV EC could initiate a differentiation process, transiting through Lrg1+ gCap before ending up to physiological gCap **(Fig. 5G)**. This inferred trajectory was supported by genes displaying a dynamic expression profile according to latent time, either progressively decreasing (*Smad1, Sparc, Col4a1, Ndrg1, Igfbp7*), transiently upregulated (*Ackr3, Emp1, Cmah, Vwf, Smad7*), or progressively increasing (Npr3, Hpgd, Clec1a, Bmp6, Itga1) (**Supplemental fig. S6B-C**. This trajectory was similarly proposed in the same configuration in the old mice 28 days after instillation (**Supplemental fig. S6D)**. We thus hypothesize that in the bleomycin reversible fibrosis model, SV EC are recruited to contribute to gCap replenishment and to the regeneration of the lung capillary endothelium integrity while in the human pathology, SV EC are not able to differentiate and accumulate, contributing to persistent fibrosis.

## DISCUSSION

In this work, we used scRNA-seq combined with spatial transcriptomics to follow the transcriptomic modifications of lung cell populations during fibrosis formation and resolution in a mice model of lung fibrosis. We specifically focused on the transcriptomic alterations correlated with a delayed fibrosis resolution in aged mice and identified several aging-associated changes in some PCEC subpopulations, including aCap and gCap, shifting towards a pro-angiogenic phenotype expressing Lrg1 and associated with alveolar niche regeneration. We also found that aging altered the transcriptome of gCap in control mice, with a signature suggestive of a pro-fibrotic and pro-inflammatory state. Because PCEC are intimately connected to alveolar epithelial cells and fibroblasts in the alveolus, age-associated defects in the PCEC differentiation may likely participate in the dysfunction of other cells in the alveolar niche and impede alveolar regeneration. Overall, our work indicates that age-associated transcriptomic alterations in specific PCEC subpopulations may interfere with the lung progenitor differentiation associated with a normal repair process and contribute to the persistent fibrotic process typical of the human pathology.

Our study presents a whole picture of cell dynamic changes in lung from young and aged animals during fibrosis formation and resolution at 3 time points. Using several approaches, including spatial transcriptomics, we confirmed previous work showing that aged mice suffer from impaired resolution after bleomycin injury [25-27], with a delay of repair observed at day 28 following bleomycin challenge. We also confirmed by scRNA-seq that many cell populations are affected by bleomycin, including epithelial cells, fibroblasts, macrophages and endothelial cells [28, 30-34], providing a unique dataset to analyze the transcriptomic dynamic of these populations and compared it to the kinetic of the resolution process measured with histology, collagen production and spatial transcriptomic. The most prominent cell population affected by bleomycin corresponded to macrophages, confirming previous studies [30-32]. Depending on the stimulus in the microenvironment, activated macrophages contribute to fibrosis but they may play also a role in the resolution of fibrosis [51]. According to their activation status, macrophages can be divided into two major subsets: classical activation (M1, pro-inflammatory/cytotoxic) and alternative activation (M2, anti-inflammatory/wound repair). M1-like AMs are the major population in the bronchoalveolar lavage (BAL) fluid at a steady state but after bleomycin exposure, M2-like alveolar macrophages gradually increased and reached the maximum level on day 14 which correlated with collagen deposition. Using genetically

engineered in vivo models, Misharin and colleagues further highlighted the importance of Mo-AMs in the development of fibrosis, showing that Mo-AMs, but not AMs, mainly contributed to the development of lung fibrosis in response to bleomycin and TGF-β [32]. Our data confirmed and extended these observations, with a rapid drop of the Fabp1+ AM1 upon bleomycin administration along with an influx of Spp1+ Mo-AMs (AM3) at the peak of fibrosis. Interestingly, while the proportion of Mo-AMs progressively decreased during the resolution phase, we identified an intermediate population (AM2) sharing both AM1 and AM3 markers that also appeared during the fibrotic phase but then maintained stable until day 60. The dynamic of these cell pops suggests that AM2 may result from AM1 differentiation but lineage-tracing studies are required to confirm this hypothesis. Finally, we found that bleomycin challenge induced remarkably similar dynamics of these macrophage subsets in young and aged animals, strongly suggesting that aging induces minor changes in macrophages recruitment and activation in our model. These data also suggest that the inflammatory response induced by bleomycin was roughly identical in young and old mice, ruling out a potential experimental bias since the intensity of the fibrotic response generally correlates with that of the inflammatory response.

The second most affected cell type by the bleomycin challenge in our dataset corresponded to EC, with several main subpopulations that were only apparent in bleomycin-injured lungs. First, we identified an homologous Col15a1-positive SV EC population, previously described in lungs from IPF patients [16], as well as a cluster of proliferating PCEC. Secondly, we found two new subpopulations of gCap and aCap cells in fibrotic lungs sharing a partial common gene signature characterized by the overexpression of *Lrg1*. Interestingly, among these distinct populations, only Lrg1+ gCap and Lrg1+ aCap cells displayed a different kinetic profile following bleomycin challenge in young and aged mice. While they both peaked at day 14 in young mice lungs, their dynamic was strongly shifted in the lungs of aged mice, peaking at day 28. This important observation has been validated by ISH and spatial transcriptomics on an independent set of mice. Although Visium's spatial transcriptomic approach does not allow for single-cell resolution, we were able to specifically localize the delayed expression of Lrg1 at 28 days in several areas of aged mouse sections, such as alveoli and fibrotic regions. Overall, our findings demonstrate that bleomycin injury induces PCEC remodeling marked by the upregulation of *Lrg1* and the emergence of distinct capillary activated cell states that are delayed in aged mice.

*Lrg1* is a secreted member of the family of leucine-rich repeat proteins, that often served as pattern recognition motifs for the innate immune system [52]. LRG1 is a multifunctional signaling molecule initially associated with pathological angiogenesis [39] that can notably modulate the TGF-β pathway in a highly context-dependent manner. The activation of STAT3 by various cytokines and interleukins in several cell types including EC has been involved in the upregulation of LRG1 expression [53, 54], in agreement with the enrichment of pro-inflammatory signaling pathways observed in bleomycin-challenged Lrg1+ PCEC. The physiological function of LRG1 remains poorly understood, with knockout mice showing no obvious phenotypic defects. Several studies indicate that LRG1 promotes physiological wound healing and maintain tissue homeostasis [55, 56], although abnormal LRG1 expression levels has been found to disturb effective would healing and contribute to fibrosis in several tissues including lung [57]. These data suggest that Lrg1 expression must be finely regulated during the repair process and that abnormal levels of LRG1 may disrupt effective wound healing and contribute to fibrogenesis. One of the most compelling examples of LRG1 function in promoting diseased vessels is commonly described as the TGF-β angiogenic switch, which switches EC TGF-β signaling to a proliferative pathway in a variety of pathological settings, including age-related macular degeneration and cancer. While binding of TGF-β to endothelial TGF-β type II receptor (TGFβRII) normally initiates signaling through the tyrosine kinase receptor ALK5 coupled to Smad2/3, preserving cell quiescence, high levels of LRG1 can redirect TGF-β to form a transduction complex with ALK1 and the accessory receptor endoglin (ENG), activating the pro-angiogenic Smad1/5/8 pathway and promoting EC proliferation, migration and tubulogenesis as well as the expression of several pro-angiogenic factors such as VEGFA. This mechanism may likely explain our data showing inhibition of endothelial quiescence in

gCap Lrg1+ as well as strong induction of markers associated with EC proliferation and migration after lung injury to promote angiogenesis and sprouting. While this destabilizing Lrg1-associated pro-angiogenic activity appears to be necessary to promote alveolar vascular repair, prolonged expression of Lrg1 in aged mice could be rather angiopathic, preventing the formation of a mature capillary network thus causing tissue malfunction.

The Lrg1-associated gene signature found in our study also contains Sox17, a member of the Sry-related high mobility group domain family F (Sox F) transcription factors, a key developmental regulator of EC lineage. Previous work indicated that induction of Sox17 expression through the activation of HIF-1α in EC plays an essential role in regenerating EC following endotoxin-induced EC injury, notably by transcribing Cyclin E1 and stimulating proliferation of EC [58]. Of note, both *SOX17* and *HIF1A* were also detected in PCEC in lungs from IPF patients, indicative of a pro-angiogenic activity. The activation of a hypoxic response was particularly visible in Lrg1+ aCap and Lrg1+ gCap with several markers associated with glycolysis and hypoxia, in agreement with studies indicating that transient activation of hypoxia-mediated signaling pathways contributed to angiogenesis and vascular repair [59, 60]. In addition to hypoxia, our analysis revealed transcriptomic modulations of mTOR, TGF-β, IL-8 and integrin-linked kinase signaling and related notably to vasculogenesis, sprouting, cell-cell contact, cell migration and inflammation. The identification of multiple cytokines/growth factors and receptors in activated PCEC suggested extensive heterotypic interactions within the alveolar niche. Our ligand-receptor interaction predictions propose a complex network of interactions involving ligands expressed by activated PCEC and neighboring cell types within the alveolar niche, including AT1, AT2, mesenchymal cells as well as mast cells, neutrophils and macrophages that likely influence alveolar repair. Remarkably, some of these predictions are in agreement with previous studies highlighting in particular the importance of the signaling pathway involving *Cxcl12* (also known as SDF-1) and *Ackr3* (Cxrc7) in PCEC, leading to neo-alveolarization [42]. Further work is needed to analyze the functional importance of this predicted network and to characterize their central regulators with the goal to potentially target specific signaling pathways within the vascular niche for regenerative therapies.

After having shown a difference in the dynamics of Lgr1+ PCEC following lung injury between aged and young animals, we then focused on additional transcriptomic differences in these populations in physiological or pathological conditions. We particularly focused on gCap population that functions as progenitor cell for aCap in capillary homeostasis and repair [12]. We found that in lungs from aged bleomycin-challenged mice, gCap expressed an enriched pro-inflammatory signature including genes from the S100 family and the antigen presentation pathway, as well as decreased expression levels of several transcription factors associated with vascular homeostasis, repair and the anti-inflammatory response (*Klf2, Peg3, Klf10)* [44-46], indicating that the bleomycin response was exacerbated in gCap from aged mice. In addition, we also found an aging-related signature in gCap from healthy control lungs. Part of this signature (21 genes), corresponding mostly to genes associated with angiogenesis, migration and sprouting, was correlated with the bleomycin-induced signature, suggesting a pre-inflammatory and pre-fibrotic cell state in old gCap. A significant portion of the signature was also consistent with inflammatory and antigen presentation pathways, in agreement with an increased expression of the class II transactivator (CIITA), a positive regulator of MHC-II molecules transcription. Emerging evidence suggest a tissue-specific and vessel type-specific immunomodulatory role for distinct subtypes of EC, referred to as immunomodulatory EC (IMEC) [61, 62]. Several studies indicate that lung PCEC specifically express MHC-II expression [63, 64] and recent single-cell approaches indicated that gCap can activate CD4+ T cells through MHC-II, suggesting that they are involved in immune cell recruitment and in controlling a delicate balance between immunity and tolerance to pathogens [12] or autoantigens. Mechanisms involved in EC dysfunction during aging are poorly understood. A pioneer single-cell atlas of the aging lung [65] pointed to an upregulation of various cytokine transcripts, such as Il1b, Tnf and Tgfb1 in PCEC from aged mice, suggesting that capillaries might contribute to lung diseases that are more prevalent in elderly people, such as chronic obstructive pulmonary disease and IPF, and might also contribute to the severity of COVID-19 [66]. Another recent study reported a widespread reduction of chromatin accessibility in EC

from aged lungs resulting in limited expression of genes involved in angiogenesis and vascular remodeling [19]. The endothelial transcription factor ERG was proposed as a key orchestrator of gCap EC repair and its dysfunctional signaling with aging was found to impair alveolar capillary regeneration, resulting in paracrine fibroblast activation and persistent fibrosis. Our data are in agreement with these different studies and extend some hypotheses proposing that ageing affects immunomodulation by capillary EC via alterations of various pathways involved in immune cell recruitment and antigen processing. In particular, our data indicating an aging-dependent activation of the antigen presentation pathway in gCap is in agreement with the defects of autoimmunity largely described in IPF patients [67, 68]. Indeed, lung sections from IPF patients often show large lymphocyte aggregates composed of CD3+ T cells and CD20+ B cells and autoantibodies to a range of host antigens have been detected in IPF patients, suggesting a breakdown in immunological tolerance. Future studies in mice targeting the MHC-II pathway are needed to gain a functional understanding of how dysregulation of the immune response may exacerbate disease progression in IPF.

Although the mouse models of IPF may not accurately reflect on the vascular alterations observed in IPF patients, we compared our data with a public IPF scRNA-seq dataset published by Habermann et al [48]. As previously described [16], IPF samples were characterized by the emergence of a COL15A1+ SV EC populations and these data were confirmed on lung IPF sections using the pan-endothelial marker anti-CD31 and anti-COL15A1. While *LRG1* transcript was expressed at a low level in this population, we found a large common signature of 218 genes between fibrotic mouse and human samples in SV EC, indicating that the pulmonary endothelial remodeling observed after bleomycin-induced lung injury in mice mimics the recruitment of SV EC occurring in IPF. In contrast, the aCap lrg1+ and gCap Lgr1+ populations were not clearly detected in IPF samples and only a small fraction of genes appeared to be commonly modulated in aCap / gCap populations from fibrotic lungs in humans and mice. However, we could detect a significant expression of LRG1 at the protein level in the majority of CD31+ cells exclusively in IPF samples. The characterization of EC heterogeneity in IPF is still in its infancy. In particular, it is not known whether the ectopic presence of COL15A1+ SV EC in the IPF-associated distal parenchyma, play a role in the pathogenesis of IPF. In order to gain information on their potential function, we used our scRNA-seq dataset on young PCEC at day 14 to investigate the potential relationship between SV EC and gCap using the RNA velocity approach [50]. Our results indicate that following lung injury SV EC are recruited and function as progenitor cells that can initiate a differentiation process, transiting through Lrg1+ gCap before reaching the physiological gCap cell state. The same differentiation scheme was also found in the old mice but with a delayed kinetic (28 days). Overall, these data strongly suggest that in a reversible fibrosis model (mouse), SV EC are recruited and can act as progenitor cells to reconstitute the gCap pool and regenerate the integrity of the alveolar endothelial capillaries while aging appears to delay this resolution process. It is therefore tempting to hypothesize that in the context of the human pathology, SV EC are deficient in this differentiation process and accumulate in the injured tissue. Interestingly, a recent preprint, using an *ex vivo* human precision-cut lung slice (hPCLS) model of lung fibrogenesis, also described a transcriptomic proximity between alveolar PCEC and a systemic venous EC state [69]. In this case, the authors presented a differentiation trajectory in the opposite direction, proposing that PCEC in injured alveoli give rise to a VWA1+/PLVAP+ ectopic EC state with transcriptional similarities to the systemic vasculature. Additional analyses are thus needed to better characterize this ectopic EC state versus the COL15A1+ SV EC and distinguish between these two hypotheses. Future work is also necessary to better define the molecular pathways involved in this differentiation process as well as the potential consequences of age-related alterations on this process.

During the preparation of this manuscript, Raslan et al. posted a preprint also investigating the bleomycin-induced lung injury response in young and aged mice at single-cell resolution [70]. Interestingly, they also isolated a sub-population of gCap EC marked by the expression of Ntrk2 / TrkB (Tropomyosin Receptor Kinase B) that appeared in bleomycin-injured lungs and associated with aberrant YAP/TAZ signaling, mitochondrial dysfunction, and hypoxia. These cells exhibited a similar gene expression signature as those we present here, including the

upregulation of Lrg1. However, their conclusions, stating that this population is dysfunctional and accumulates with aging, differ from ours (ie: rather a pro-regenerative pop delayed in aged animals) primarily because they study only a single time point (day 30), without considering the dynamic of appearance and disappearance of this population at earlier and later times.
Altogether, our findings shed new light into the molecular mechanisms associated with alveolar endothelial capillaries resolution in a mouse model of reversible lung fibrosis and how aging influences specific PCEC to delay this resolution process. In particular, they raise new hypotheses regarding the functional importance of these specific PCEC populations in lung repair, which may lead to new therapeutic strategies for the treatment of IPF.

**Acknowledgements:** The authors thank the technical support of the UCA GenomiX and MICA imaging platforms of the University Côte d'Azur. We also thank the staffs from the Nice Hospital-Integrated Biobank (BB-0033-00025) and the Giessen PNEUMObank as well as from the animal care facilities institutions at Sophia Antipolis (IPMC Animal Care Facility) and Lille (High Technology Animal Care Facility, University of Lille 2). We also thank Thomas Bertero and all the members of the team for fruitful discussions.

**Funding:** we acknowledge the support from the Centre National de la Recherche Scientifique (CNRS), Institut National de la Santé et de la Recherche Médicale (Inserm), Université Côte d'Azur, Université de Lille, the French Government (National Research Agency, ANR): program reference ANR-PRCI-18-CE92-0009-01 FIBROMIR and ANR-22-CE17-0046-01 MIR-ASO), Programme Contrat Plan État Région (CPER) - CTRL (Centre Transdisciplinaire de Recherche sur la Longévité, projet FISSURE) as well as Cancéropôle PACA.

**Author contributions.**
BM, NP, GV and CC conceived and designed the study and supervised the entire work. MT and BM wrote the manuscript. GS, HC and AB performed in vivo studies. GS, HC, JF and CS performed biochemical and cellular biology experiments. GS, CdS and MJA performed the Visium spatial transcriptomic experiment. VM and CGR generated scRNA-seq data and primary analysis. MT performed bioinformatic analysis of scRNA-seq and spatial transriptomic data. KLB co-supervised the computational analysis. GS, RL and HC performed and analyzed immunostainings. MT, GS, GV, CC, NP and BM performed biological interpretation. VH, PH, AG, AL and SL provided IPF-derived biological materials and contributed to biological interpretation of data. MG, RR, MP, NR, PB and SB gave conceptual advices. OP and SB provided ressources. All authors read and corrected the final manuscript.

**Competing interests.**
None declared

**Keywords :** pulmonary fibrosis, capillary endothelial cell, single-cell-RNA seq, spatial transcriptomic

## MATERIALS AND METHODS

### Reagents and antibodies

Bleomycin was obtained from Sigma Aldrich (B1141000). The following antibodies were used in immunofluorescence experiments: Mouse Anti-Human CD31 (550274 BD Biosciences), Rabbit Anti-Human LRG1 (ab231188 Abcam), Rabbit Anti-Human COL15A1 (PA5-115179 Invitrogen), Purified Mouse Anti-Actin αSMA– FITC (F3777 Sigma-Aldrich), donkey DyLight 594 Anti-Rabbit IgG (A32754 Life Technologies), donkey DyLight 647 Anti-Mouse IgG (A31571 Life Technologies).

### Mouse experiments

***Experimental design and animal treatment.*** All animal care and experimental protocols were conducted according to European, national and institutional regulations (Protocol numbers: 00236.03 and APAFIS#31298, IPMC approval E0615252; Protocol Number APAFIS#12540, University of Lille; approval 00236.03 CNRS). Personnel from the laboratory performed all experimental protocols under strict guidelines to ensure careful and consistent handling of the mice. Seven-week ("young") and 18-month ("old")-old C57BL/6 male mice (Charles River) were divided randomly into two groups: (A) saline-only (PBS, n=3), or (B) bleomycin (Bleo, n=3). To induce fibrotic changes, 50-µl bleomycin (1 U/kg) or PBS was aerosolized in mouse lungs using a MicroSprayer Aerosolizer (Penn-Century, Inc.) as previously described [71]. Mice were sacrificed at designated time points (days 14, 28 and 60) after instillation.

***Histopathology.*** Mouse lungs were fixed overnight with neutral buffered formalin and then embedded in paraffin. 5-micrometer-thick sections were mounted and stained with hematoxylin and eosin (HE) as well as Sirius Red to assess the degree of fibrosis. HE sections were scanned using Axio Scan Z1 scanner (Zeiss) at x10 magnification. Data are processed using the Zen blue imaging software (Zeiss). Hematoxylin and eosin zoomed in pictures were performed using Axiophot 2 light microscope.

***Hydroxyproline quantification of mouse lungs.*** Lung hydroxyproline content was assayed as previously described [71]. Briefly, lungs were disrupted in liquid nitrogen and 10 mg were homogenized in 100 µl of water. Samples were hydrolyzed for 3 hours at 120°C in a temperature-controlled heating block after adding 100 µl of HCl 12M and then dried. Hydroxyproline quantification was finally performed in microplate as described by the manufacturer (Sigma).

***Lung dissociation and cell preparation for Chromium™ scRNA-seq.*** Lung single cell suspensions were generated as previously described [65]. Briefly, after euthanasia, lung tissue was perfused with sterile saline through the heart and were inflated through the trachea with dissociation cocktail containing dispase (50 caseinolytic U/ml), collagenase (2 mg/ml), elastase (1 mg/ml), and DNase (30 µg/ml). Lung were immediately removed, minced to small pieces ~1mm$^3$), and transferred for mild enzymatic digestion for 20–30 min at 37 °C in 4 ml of the dissociation cocktail. Enzymatic activity was inhibited by adding 5 mL of PBS supplemented with 10% fetal calf serum (FCS). Single cells suspensions were passed through a 40-micron mesh, and then harvested by centrifugation at 300 g for 5 min (4°C). Reb blood cell lysis was performed using RBC lysis buffer (Thermo fisher) for 2 min at 4°C and stopped using PBS 10% FCS. After another centrifugation at 300g for 5 min (4°C) cells were counted and critically assessed for single cell separation and overall cell viability using the Countess 3 FL (Fisher Scientific). Samples were then stained for multiplexing using cell hashing [29], using the Cell Hashing Total-Seq-A™ protocol (Biolegend) following the protocol provided by the supplier, using 6 distinct Hash Tag Oligonucleotides-conjugated mAbs (3 PBS and 3 Bleo). Briefly 1.10$^6$ cells were resuspended in 100µl of PBS, 2% BSA, 0.01% Tween and incubated with 10µl Fc Blocking reagent for 10 min 4°C then stained with 0.5µg of cell hashing antibody for 20 minutes at 4°C. After washing with PBS, 2% BSA, 0.01% Tween samples were counted and merged at the same proportion, spun 5 minutes 350 x g at 4°C and resuspended in PBS supplemented with 0.04% of bovine serum albumin at final concentration of 500 cells/µl. Samples were then adjusted to the same concentration, mixed in PBS supplemented with 0.04% of bovine serum albumin at a final concentration of 100 cells/µl and pooled sample were immediately loaded on Chromium.

**Tissue preparation for the Visium™ spatial transcriptomics protocol.** Tissue preparation and slides processing was performed according to the Visium Tissue Preparation Guide (CG000238 Rev A; CG000239 Rev A; CG000240 Rev A, 10× Genomics). Briefly, lungs of bleomycin-challenged mouse were inflated with diluted Optimal Cutting Temperature (OCT), gently removed from mouse then embedded in OCT on dry ice and stored at -80°C. OCT blocks were cryosectioned at 10µm thickness on capture areas of Visium 10 Genomics slide. Before performing the complete protocol, Visium Spatial Tissue Optimization was performed according to manufacturer's procedure and using the Axioscan 7 scanner (Zeiss). Thirty minutes was selected as optimal permeabilization time. The experimental samples were fixed, stained with H&E and imaged using Axioscan 7 scanner at 5x magnification.

**RNA-FISH.** RNAscope probes against mmu-Lrg1 (ID: 423381), mmu-Aplnr (ID: 436171) and mmu-Ednrb (ID: 473801) were prepared and obtained from Advance Cell Diagnostics. FISH assays were performed on FFPE lung sections, as previously described [71] using Multiplex Fluorescent Reagent Kit V2 (Advanced cell Diagnostics) and TSA Plus Cyanine 3 and Cyanine 5 (Perkin Elmer) as fluorophores according to manufacturer's recommendations. Acquisition was performed using an inverted confocal microscope LSM 710 (Zeiss) and a 40x oil immersion lens.

**Generation of single cell librairies, 10X Genomics scRNA-seq and data processing.** Single-cell capture was performed using the 10X Genomics Chromium device (3′ V3). Single-cell libraries were sequenced on the Illumina NextSeq 500. Alignment of reads from the single cell RNA-seq library and unique molecular identifiers (UMIs) counting were performed with 10X Genomics Cell Ranger tool (v3.0.2). Reads of oligonucleotides tags (HTOs) used for Cell Hashing were counted with CITE-seq-Count (v1.4.2). Counts matrices of total RNA and HTOs were thus obtained for the 6 sequencing run, respectively named YoungD14, YoungD28, YoungD60, OldD14, OldD28 and OldD60.

**Single cell data secondary analysis.** All downstream analyses were carried out with Seurat R package (v4.1.0).
***HTOs demultiplexing*.** For each 6 sequencing run, RNA and HTOs counts matrices were integrated into a Seurat object. HTOs counts were demultiplexed with HTODemux() function to assign mice-of-origin for each cell (3 PBS-treated and 3 Bleomycin-treated). Only the cells identified as "Singlet" and passing quality control metrics (UMIs and mitochondrial content arbitrary thresholds adjusted according to each sample) were kept for each Seurat object. The 6 seurat objects containing the raw counts of filtered cells and their metadata (age, day of lung collection post injection, treatment, mice-of-origin) were merged.
***Samples integration*.** The computational integration of the different samples was performed using reciprocal PCA, as described in the dedicated vignette from Satija lab website (https://satijalab.org/seurat/articles/integration_rpca.html). Briefly, a "detailed samples" metadata column was created by aggregating age, day of lung collection post injection and treatment (ex: Young.D14.Bleo, Young.D14.PBS, etc). According to this "detailed samples" metadata, cells were split into 12 seurat objects. For each of 12 datasets, raw counts were normalized using SCTransform() with Gamma-Poisson generalized linear model to estimate regression parameters. 3000 features were selected for being repeatedly variable across the 12 datasets. The sctransform residuals corresponding to the selected 3000 features were computed if they were missing in a particular object. Principal Component Analysis (PCA) was run individually for each object on the sctransform normalized counts of the 3000 selected features. A set of common anchors were found among the selected features, in dimensionally reduced data by reciprocal PCA, using FindIntegrationAnchors() function with the following arguments: normalization.method = "SCT", dims = 1:50, k.anchor = 5. This set of anchors was used to create a combined object containing integrated data using 50 dimensions for the anchor weighting procedure.

***Clustering and annotation*.** First, PCA was run on the integrated data. UMAP and kNN clustering were computed on the first 80 computed principal components (PCs). Clusters corresponding to aggregates of cells sharing a low-UMIs content were discared. The entire integration and clustering processes were rerun on the cleared dataset, following the exact steps described above. The finally obtained clusters were annotated on the basis of the expression of their specific markers listed in the output of the FindAllMarkers() function.
*Differential expression analyses between fibrotic and PBS conditions in all cell populations.* Differential expression analyses between cells from bleomycin and PBS treated mice were carried out with DESeq2 (v1.30.1). First, all counts of each cell population from the same mice were aggregated to create a pseudobulk sample. For the PBS condition, we thus systematically obtain 18 pseudobulks samples corresponding to the 3 young and 3 old PBS-treated lungs collected at day 14, at day 28 and at day 60. For the fibrotic condition, we excluded the samples from bleomycin-treated lungs collected at day 60, which correspond to an almost complete fibrosis resolution. We thus obtained 12 pseudobulks corresponding to the 3 young and 3 old bleomycin-treated lungs collected at day 14 and at day 28. For the alveolar macrophages pseudobulks, all counts from the 3 subpopulations (AM1, AM2, AM3) were aggregated. For gCap and aCap pseudobulks, all counts of gCap plus Lrg1+ gCap or aCap plus Lrg1+ aCap were aggregated. Genes considered as differentially expressed were selected according to an adjusted pvalue threshold of 0.05, obtained with the Wald test and the Benjamini-Hochberg method for multiple tests correction implemented in DESeq2.

**Detailed analysis of endothelial cells (EC).**
***Identification of EC subpopulations.*** The clusters corresponding to general capillary cells (gCap) and aerocytes (aCap) were extracted and subclustered using the 80 PCs already computed from the integrated assay of the complete dataset. Clusters corresponding to Lrg1+ aCap, Lrg1+ gCap and SV EC subpopulations were added to the annotation and UMAP was rerun on the subset of cells corresponding to gCap, aCap, proliferating EC, Lrg1+ aCap, Lrg1+ gCap, SV EC, PV EC and Arterial EC using the same number of dimensions. The original raw counts were finally log-normalized with NormalizeData for all data exploration and visualization.
***Relative subpopulations frequencies*.** All PBS-treated mice with the same age and sacrificed at D14, D28 or D60 were considered as replicates (n=9), while Bleomycin-treated mice were separated according to age and time of sacrifice (n=3 for each time point). The relative subpopulations frequencies at the 4 time points (PBS, D14, D28, D60) were obtained by calculating the ratio between the number of cells in each EC subpopulation and the total number of EC in each mice replicate, either mixing or distinguishing young and old mice.
*Percentage of expression of genes*. The percentage of expression of genes in a particular subset of EC subpopulations, at a particular time point, in young or old mice, were obtained by calculating the ratio between the number of cells of the particular subset expressing at least 1 UMI of the specific gene and the total number of cells of the particular subset.
*Bleomycin-induced fibrosis score*. To compute a bleomycin-induced fibrosis score in gCap, aCap and PVEC, only the most significant upregulated genes from the differential expression analyses described above were selected according to adjusted pvalue (<0.05), log2FoldChange (>0.5) and base mean expression (>10 for gCap, >5 for aCap and PV EC). Lists of selected genes were used to compute a score at the single cell level using the AddModuleScore() function. Scores were finally compared between the 4 time points (PBS, D14, D28, D60) and between young or old animals.
***Comparison between old vs young gCap in fibrotic and physiological conditions*.** To compare the transcriptomic profiles of gCap from old and young mice in fibrotic condition, counts from bleomycin-treated gCap and Lrg1+gCap were aggregated within the same mouse for day 14 and day 28 timepoints, in order to obtain 6 young and 6 old pseudobulks samples. The same process has been applied to build pseudobulk samples of physiological gCap but including day 60 samples, resulting in 9 pseudobulks for either young of old groups. Differential analysis between old and young pseudobulks samples were carried out with DESeq2

(v1.30.1). DEGs were selected according to adjusted pvalue (<0.05), absolute log2FoldChange (>0.5) and base mean expression (>5).
*SV EC transcriptomic signature in fibrotic condition*. As SV EC from control samples were poorly detected either in mouse or human data, SV EC from fibrotic conditions were compared to control SV EC plus control PV EC using the pseudobulk-based approach.
***Ingenuity Pathway Analysis.*** To investigate the enriched pathways and functions associated to DEGs either in the fibrotic versus control comparison or old versus young comparison, we used the core analysis of the Ingenuity Pathway Analysis tool (IPA, Ingenuity® Systems, www.ingenuity.com) using the results of the treatment (bleomycin)- or aging-perturbed genes obtained by DGE testing (see above) as input..

**RNA velocity analyses.** The RNA velocity analyses were carried out following the kallisto | bus (https://bustools.github.io/BUS_notebooks_R/velocity.html) and scVelo workflows (https://scvelo.readthedocs.io/).
***Generation of spliced and unspliced matrices.*** Intronic sequences of the mouse genome assembly GRCm38 were first identified using the get_velocity_files () function of the BUSpaRse R package (v1.5.2) and the gencode annotation (v.M25). In order to allow the pseudoalignment of reads on both cDNA and identified intronic sequences, indexes for both cDNA and intronic sequences were built using kallisto (v0.46.2). The spliced and unpliced matrices were then generated for each sequencing run using the wrapper combining kallisto and bustools (v0.39.2) functions, typically with the following command line: kb count -i mm_cDNA_introns_index.idx -g tr2g.tsv -x 10xv3 -o kb \
-c1 cDNA_tx_to_capture.txt -c2 introns_tx_to_capture.txt --workflow lamanno \
sample_x_L001_R1_001.fastq.gz sample_x_L001_R2_001.fastq.gz \
sample_x_L002_R1_001.fastq.gz sample_x_L002_R2_001.fastq.gz \
sample_x_L003_R1_001.fastq.gz sample_x_L003_R2_001.fastq.gz \
sample_x_L004_R1_001.fastq.gz sample_x_L004_R2_001.fastq.gz
***Preprocessing***. Generated spliced and unspliced matrices of each sequencing run were then preprocessed to filtered out empty droplets, to remove undetected genes and to replace ensembl IDs by gene symbols. Spliced and unspliced matrices corresponding to barcodes of subset of cells of interest, for example SV EC, Lrg1+ gCap and gCap from Bleomycin and PBS-treated mice at day 14, were integrated in a seurat object. The spliced raw counts were normalized using SCTransform() from seurat R package, and PCA was run on these normalized data , as well as UMAP with the first 30 PCs. The seurat object was then converted to .h5ad file, keeping only the two raw spliced and unspliced assays.
***RNA velocity using scVelo***. The .h5ad file was read to an AnnData object using scVelo python package (v0.2.4). Again, data were preprocessed: the counts of the 3000 most variable genes with at list 20 reads were log-normalized using the filter_and_normalize() function. PCA and nearest neighbors were computed before the estimation of velocity. The full transcriptional dynamics of splicing kinetics was resolved using the generalized dynamical model and represented as latent time in each cell.

**NicheNet analysis.** We used the nichenet R package (v1.0.0) to infer ligand-receptor interaction candidates able to induce the expression of pro-angiogenic genes in SV EC, Lrg1+ gCap and Lrg1+ aCap cells. For each of this 3 subpopulations, alternatively considered as receiver cells, we computed the activities of ligand sent by all the detected populations of the whole dataset. As genesets, we alternatively used the pro-angiogenic genes expressed in at least one third of cells with an average expression above 1 in the particular subpopulation. For each ligand activities computed for each subpopulation, we selected the top 14 most likely to induce the geneset of interest by ranking them according to Pearson's correlation coefficient. The union of the 3 lists of prioritized ligands resulted in the 17 ligands used for the visualization. The selected receptors of those 17 ligands were only those considered as "bona fide", i.e. those whose interaction with their ligand is not only predicted in silico. The only exception is for Apoe which didn't have a bona fide receptor according to the NicheNet model, for which its best predicted receptor Scarb1 was added. The circos plot linking prioritized ligands and their

receptors was realized following the steps described in the dedicated nichenet's vignette (https://github.com/saeyslab/nichenetr/blob/master/vignettes/circos.md).

**Generation of Visium spatial transcriptomic libraries.**
Library preparation was performed according to the Visium Spatial Gene Expression User Guide. Libraries were loaded and sequenced on a NextSeq2000 System (Illumina) as paired-end-dual-indexed, at a sequencing depth of approximately 25 M read-pairs per capture area.

**Analysis of spatial transcriptomics data.** The 8 spaceranger pipeline outputs containing both the spot-level gene counts and the histological image of the tissue slice were read as seurat objects. After a quick overview of each one, 2 of them (Young.D14_bis and Young.D28_bis) appeared unusable because of a very low level of detected molecules per spot (<800 detected genes). The remaining 6 samples (Young.D14, Old.D14.a, Old.D14.b, Young.D28, Old.D28.a, Old.D28.b) were first normalized with SCTransform(). PCA was run in each sample using the intersection of the top 10000 variable features found in each sample. The 6 samples were then integrated by reciprocal PCA following the same steps than described for the scRNA seq samples integration. The clusters obtained in the PCA-reduced space from integrated data were annotated on the basis of their differentially expressed markers obtained with the FindAllMarkers() function. Percentage and level of Lrg1 expression in the annotated zones of each slice and their relative frequencies were obtained in the same way as for the scRNA seq data.

**Re-analysis of public scRNA-seq datasets.** Both human lung fibrosis (Habermann et al.) and mouse lung public dataset (Strunz et al.) were re-analysed, using reciprocal PCA as already described, in order to integrate samples from different patients or different mice. To reduce the complexity of the human lung fibrosis dataset, we only kept cells coming from either IPF-diagnosed or normal samples and we randomly sampled 10000 immune cells and 5000 epithelial cells. Adding the total number of endothelial and mesenchymal cells, we obtained a dataset of 25816 cells. Differential expression analyses between pulmonary endothelial cells from IPF and control samples were obtained with the same pseudobulk-based strategy described above.

**IPF lung tissue sections.** Lung tissue sections were obtained from the UGMLC Giessen Biobank affiliated to the European IPF Registry as well as from the Nice Hospital-Integrated Biobank.

**Immunohistochemistry and Immunofluorescence microscopy**. 5-µm paraffin-embedded sections were sequentially incubated in xylene (5 min twice), 100% ethyl alcohol (5 min twice), 95% ethyl alcohol (5 min twice), and 80% ethyl alcohol (5 min) and H&E stained as previously described [71]. After washing with water, the sections were antigen-retrieved using citrate buffer (pH 6.0; Sigma-Aldrich) in a domestic microwave oven for 15 minutes and cooled to ambient temperature. Autofluorescence was quenched for 20-30 minutes and passed in Photobleacher for 1h30. Slides were incubated with the primary antibodies (dilution 1:200, anti-CD31, anti-LRG1; anti-COL15A1, Anti-SMA–FITC) diluted in a blocking solution BSA (1%) over night at 4°C. Slides were incubated for 1h with secondary antibodies (dilution 1:200) at room temperature. Then slides were incubated for 15 min with Dapi (dilution 1:5000) (D1306 Life Technologies). Slides were mounted using Immu-Mount (9990414 Fisher scientific). Representative regions of stained slices were digitalized on a epifluorescent Zeiss and analyzed using the software ImageJ.

**Statistical Analysis.** Cell type–specific marker genes were established using the Wilcoxon rank sum test with P values adjusted for multiple comparisons using the Bonferroni method. Adjusted P values <0.05 were considered significant. Statistical analyses were performed using GraphPad Prism. Results are given as mean±S.E.M. Two-tailed Mann–Whitney test was used for single comparisons; one-way ANOVA controlling the false discovery rate (FDR) using

Benjamini–Hochberg procedure was used for multiple comparisons. P-value <0.05 was considered statistically significant.

**Data availability**. The scRNA-seq and spatial transcriptomic data sets have been deposited in the Gene Expression Omnibus SuperSerie GSE234199. The data are available on request and will be made publicly available once the manuscript has been accepted for publication.

**Code availability.** The scripts used for the figures will be available on github (https://github.com/marintruchi) by the time of publication.

## Supplementary material

***Correspondence of supplementary tables:***
**Supplementary table 1:** Differential expression analysis (Seurat) between annotated clusters of spatial transcriptomic data.
**Supplementary table 2:** Differential expression analysis (Seurat) between annotated subpopulations of single cell RNA-seq data.
**Supplementary table 3:** Differential expression analysis (DESeq2) between bleomycin-treated and PBS-treated cells.
**Supplementary table 4:** Differential expression analysis (DESeq2) between old and young aCap or gCap cells in fibrotic condition.
**Supplementary table 5:** Differential expression analysis (DESeq2) between old and young aCap or gCap cells in physiological condition.
**Supplementary table 6:** Differential expression analysis (DESeq2) between IPF and control aCap, gCap, SV EC and PV EC from Habermann et al.

***Supplementary Figures***
**Supplemental Figure S1:** Histological and spatial transcriptomics data integration of injured lung slices from young and old mice.
**Supplemental Figure S2:** Details on macrophages subpopulations kinetics, SV EC markers and Lrg1 expression.
**Supplemental Figure S3:** Bleomycin-induced CEC subpopulations are associated to pro-angiogenic signalling.
**Supplemental Figure S4:** Expression of bleomycin induced genes in capillary endothelial cells in single cell RNA-seq and spatial transcriptomics data.
**Supplemental Figure S5:** RNA scope time series.
**Supplemental Figure S6:** SVEC subpopulation dynamics in mouse fibrosis.

## References


1. Hogan BL, Barkauskas CE, Chapman HA, Epstein JA, Jain R, Hsia CC, Niklason L, Calle E, Le A, Randell SH, Rock J, Snitow M, Krummel M, Stripp BR, Vu T, White ES, Whitsett JA, Morrisey EE. Repair and regeneration of the respiratory system: complexity, plasticity, and mechanisms of lung stem cell function. *Cell Stem Cell* 2014: 15(2): 123-138.
2. Zepp JA, Morrisey EE. Cellular crosstalk in the development and regeneration of the respiratory system. *Nat Rev Mol Cell Biol* 2019: 20(9): 551-566.
3. Lederer DJ, Martinez FJ. Idiopathic Pulmonary Fibrosis. *N Engl J Med* 2018: 378(19): 1811-1823.
4. Wijsenbeek M, Cottin V. Spectrum of Fibrotic Lung Diseases. *N Engl J Med* 2020: 383(10): 958-968.
5. Spagnolo P, Kropski JA, Jones MG, Lee JS, Rossi G, Karampitsakos T, Maher TM, Tzouvelekis A, Ryerson CJ. Idiopathic pulmonary fibrosis: Disease mechanisms and drug development. *Pharmacol Ther* 2021: 222: 107798.
6. Wolters PJ, Collard HR, Jones KD. Pathogenesis of idiopathic pulmonary fibrosis. *Annu Rev Pathol* 2014: 9: 157-179.
7. Lopez-Ramirez C, Suarez Valdivia L, Rodriguez Portal JA. Causes of Pulmonary Fibrosis in the Elderly. *Med Sci (Basel)* 2018: 6(3).
8. Mora AL, Bueno M, Rojas M. Mitochondria in the spotlight of aging and idiopathic pulmonary fibrosis. *J Clin Invest* 2017: 127(2): 405-414.
9. Cho SJ, Stout-Delgado HW. Aging and Lung Disease. *Annu Rev Physiol* 2020: 82: 433-459.
10. Venosa A. Senescence in Pulmonary Fibrosis: Between Aging and Exposure. *Front Med (Lausanne)* 2020: 7: 606462.
11. Alvarez DF, Huang L, King JA, ElZarrad MK, Yoder MC, Stevens T. Lung microvascular endothelium is enriched with progenitor cells that exhibit vasculogenic capacity. *Am J Physiol Lung Cell Mol Physiol* 2008: 294(3): L419-430.
12. Gillich A, Zhang F, Farmer CG, Travaglini KJ, Tan SY, Gu M, Zhou B, Feinstein JA, Krasnow MA, Metzger RJ. Capillary cell-type specialization in the alveolus. *Nature* 2020: 586(7831): 785-789.
13. Ding BS, Nolan DJ, Guo P, Babazadeh AO, Cao Z, Rosenwaks Z, Crystal RG, Simons M, Sato TN, Worgall S, Shido K, Rabbany SY, Rafii S. Endothelial-derived angiocrine signals induce and sustain regenerative lung alveolarization. *Cell* 2011: 147(3): 539-553.
14. Vila Ellis L, Cain MP, Hutchison V, Flodby P, Crandall ED, Borok Z, Zhou B, Ostrin EJ, Wythe JD, Chen J. Epithelial Vegfa Specifies a Distinct Endothelial Population in the Mouse Lung. *Dev Cell* 2020: 52(5): 617-630 e616.
15. Niethamer TK, Stabler CT, Leach JP, Zepp JA, Morley MP, Babu A, Zhou S, Morrisey EE. Defining the role of pulmonary endothelial cell heterogeneity in the response to acute lung injury. *Elife* 2020: 9.
16. Adams TS, Schupp JC, Poli S, Ayaub EA, Neumark N, Ahangari F, Chu SG, Raby BA, DeIuliis G, Januszyk M, Duan Q, Arnett HA, Siddiqui A, Washko GR, Homer R, Yan X, Rosas IO, Kaminski N. Single-cell RNA-seq reveals ectopic and aberrant lung-resident cell populations in idiopathic pulmonary fibrosis. *Sci Adv* 2020: 6(28): eaba1983.
17. Ungvari Z, Tarantini S, Donato AJ, Galvan V, Csiszar A. Mechanisms of Vascular Aging. *Circ Res* 2018: 123(7): 849-867.
18. Xu X, Wang B, Ren C, Hu J, Greenberg DA, Chen T, Xie L, Jin K. Age-related Impairment of Vascular Structure and Functions. *Aging Dis* 2017: 8(5): 590-610.
19. Caporarello N, Lee J, Pham TX, Jones DL, Guan J, Link PA, Meridew JA, Marden G, Yamashita T, Osborne CA, Bhagwate AV, Huang SK, Nicosia RF, Tschumperlin DJ, Trojanowska M, Ligresti G. Dysfunctional ERG signaling drives pulmonary vascular aging and persistent fibrosis. *Nat Commun* 2022: 13(1): 4170.
20. Jenkins RG, Moore BB, Chambers RC, Eickelberg O, Konigshoff M, Kolb M, Laurent GJ, Nanthakumar CB, Olman MA, Pardo A, Selman M, Sheppard D, Sime PJ, Tager AM, Tatler AL, Thannickal VJ, White ES. An Official American Thoracic Society Workshop Report:

Use of Animal Models for the Preclinical Assessment of Potential Therapies for Pulmonary Fibrosis. *Am J Respir Cell Mol Biol* 2017: 56(5): 667-679.

21. Redente EF, Jacobsen KM, Solomon JJ, Lara AR, Faubel S, Keith RC, Henson PM, Downey GP, Riches DW. Age and sex dimorphisms contribute to the severity of bleomycin-induced lung injury and fibrosis. *Am J Physiol Lung Cell Mol Physiol* 2011: 301(4): L510-518.
22. Stout-Delgado HW, Cho SJ, Chu SG, Mitzel DN, Villalba J, El-Chemaly S, Ryter SW, Choi AM, Rosas IO. Age-Dependent Susceptibility to Pulmonary Fibrosis Is Associated with NLRP3 Inflammasome Activation. *Am J Respir Cell Mol Biol* 2016: 55(2): 252-263.
23. Sueblinvong V, Neujahr DC, Mills ST, Roser-Page S, Ritzenthaler JD, Guidot D, Rojas M, Roman J. Predisposition for disrepair in the aged lung. *Am J Med Sci* 2012: 344(1): 41-51.
24. Sueblinvong V, Neveu WA, Neujahr DC, Mills ST, Rojas M, Roman J, Guidot DM. Aging promotes pro-fibrotic matrix production and increases fibrocyte recruitment during acute lung injury. *Adv Biosci Biotechnol* 2014: 5(1): 19-30.
25. Hecker L, Logsdon NJ, Kurundkar D, Kurundkar A, Bernard K, Hock T, Meldrum E, Sanders YY, Thannickal VJ. Reversal of persistent fibrosis in aging by targeting Nox4-Nrf2 redox imbalance. *Sci Transl Med* 2014: 6(231): 231ra247.
26. Caporarello N, Meridew JA, Aravamudhan A, Jones DL, Austin SA, Pham TX, Haak AJ, Moo Choi K, Tan Q, Haresi A, Huang SK, Katusic ZS, Tschumperlin DJ, Ligresti G. Vascular dysfunction in aged mice contributes to persistent lung fibrosis. *Aging Cell* 2020: 19(8): e13196.
27. Rehan M, Kurundkar D, Kurundkar AR, Logsdon NJ, Smith SR, Chanda D, Bernard K, Sanders YY, Deshane JS, Dsouza KG, Rangarajan S, Zmijewski JW, Thannickal VJ. Restoration of SIRT3 gene expression by airway delivery resolves age-associated persistent lung fibrosis in mice. *Nat Aging* 2021: 1(2): 205-217.
28. Liang J, Huang G, Liu X, Liu N, Taghavifar F, Dai K, Yao C, Deng N, Wang Y, Chen P, Hogaboam C, Stripp BR, Parks WC, Noble PW, Jiang D. Reciprocal interactions between alveolar progenitor dysfunction and aging promote lung fibrosis. *Elife* 2023: 12.
29. Stoeckius M, Zheng S, Houck-Loomis B, Hao S, Yeung BZ, Mauck WM, 3rd, Smibert P, Satija R. Cell Hashing with barcoded antibodies enables multiplexing and doublet detection for single cell genomics. *Genome Biol* 2018: 19(1): 224.
30. Joshi N, Watanabe S, Verma R, Jablonski RP, Chen CI, Cheresh P, Markov NS, Reyfman PA, McQuattie-Pimentel AC, Sichizya L, Lu Z, Piseaux-Aillon R, Kirchenbuechler D, Flozak AS, Gottardi CJ, Cuda CM, Perlman H, Jain M, Kamp DW, Budinger GRS, Misharin AV. A spatially restricted fibrotic niche in pulmonary fibrosis is sustained by M-CSF/M-CSFR signalling in monocyte-derived alveolar macrophages. *Eur Respir J* 2020: 55(1).
31. Aran D, Looney AP, Liu L, Wu E, Fong V, Hsu A, Chak S, Naikawadi RP, Wolters PJ, Abate AR, Butte AJ, Bhattacharya M. Reference-based analysis of lung single-cell sequencing reveals a transitional profibrotic macrophage. *Nat Immunol* 2019: 20(2): 163-172.
32. Misharin AV, Morales-Nebreda L, Reyfman PA, Cuda CM, Walter JM, McQuattie-Pimentel AC, Chen CI, Anekalla KR, Joshi N, Williams KJN, Abdala-Valencia H, Yacoub TJ, Chi M, Chiu S, Gonzalez-Gonzalez FJ, Gates K, Lam AP, Nicholson TT, Homan PJ, Soberanes S, Dominguez S, Morgan VK, Saber R, Shaffer A, Hinchcliff M, Marshall SA, Bharat A, Berdnikovs S, Bhorade SM, Bartom ET, Morimoto RI, Balch WE, Sznajder JI, Chandel NS, Mutlu GM, Jain M, Gottardi CJ, Singer BD, Ridge KM, Bagheri N, Shilatifard A, Budinger GRS, Perlman H. Monocyte-derived alveolar macrophages drive lung fibrosis and persist in the lung over the life span. *J Exp Med* 2017: 214(8): 2387-2404.
33. Tsukui T, Sun KH, Wetter JB, Wilson-Kanamori JR, Hazelwood LA, Henderson NC, Adams TS, Schupp JC, Poli SD, Rosas IO, Kaminski N, Matthay MA, Wolters PJ, Sheppard D. Collagen-producing lung cell atlas identifies multiple subsets with distinct localization and relevance to fibrosis. *Nat Commun* 2020: 11(1): 1920.
34. Buechler MB, Pradhan RN, Krishnamurty AT, Cox C, Calviello AK, Wang AW, Yang YA, Tam L, Caothien R, Roose-Girma M, Modrusan Z, Arron JR, Bourgon R, Muller S, Turley SJ. Cross-tissue organization of the fibroblast lineage. *Nature* 2021: 593(7860): 575-579.

35. Chu X, Lingampally A, Moiseenko A, Kheirollahi V, Vazquez-Armendariz AI, Koepke J, Khadim A, Kiliaris G, Shahriari Felordi M, Zabihi M, Shalashova I, Alexopoulos I, Gunther S, Lebrigand K, Truchi M, Gunther A, Braun T, Mari B, Samakovlis C, Li X, Seeger W, Herold S, Zhang JS, Bellusci S, El Agha E. GLI1+ cells are a source of repair-supportive mesenchymal cells (RSMCs) during airway epithelial regeneration. *Cell Mol Life Sci* 2022: 79(11): 581.
36. Moiseenko A, Vazquez-Armendariz AI, Kheirollahi V, Chu X, Tata A, Rivetti S, Gunther S, Lebrigand K, Herold S, Braun T, Mari B, De Langhe S, Kwapiszewska G, Gunther A, Chen C, Seeger W, Tata PR, Zhang JS, Bellusci S, El Agha E. Identification of a Repair-Supportive Mesenchymal Cell Population during Airway Epithelial Regeneration. *Cell Rep* 2020: 33(12): 108549.
37. Mari B, Crestani B. Dysregulated balance of lung macrophage populations in idiopathic pulmonary fibrosis revealed by single-cell RNA seq: an unstable "menage-a-trois". *Eur Respir J* 2019: 54(2).
38. Schupp JC, Adams TS, Cosme C, Jr., Raredon MSB, Yuan Y, Omote N, Poli S, Chioccioli M, Rose KA, Manning EP, Sauler M, DeIuliis G, Ahangari F, Neumark N, Habermann AC, Gutierrez AJ, Bui LT, Lafyatis R, Pierce RW, Meyer KB, Nawijn MC, Teichmann SA, Banovich NE, Kropski JA, Niklason LE, Pe'er D, Yan X, Homer RJ, Rosas IO, Kaminski N. Integrated Single-Cell Atlas of Endothelial Cells of the Human Lung. *Circulation* 2021: 144(4): 286-302.
39. Wang X, Abraham S, McKenzie JAG, Jeffs N, Swire M, Tripathi VB, Luhmann UFO, Lange CAK, Zhai Z, Arthur HM, Bainbridge J, Moss SE, Greenwood J. LRG1 promotes angiogenesis by modulating endothelial TGF-beta signalling. *Nature* 2013: 499(7458): 306-311.
40. Strunz M, Simon LM, Ansari M, Kathiriya JJ, Angelidis I, Mayr CH, Tsidiridis G, Lange M, Mattner LF, Yee M, Ogar P, Sengupta A, Kukhtevich I, Schneider R, Zhao Z, Voss C, Stoeger T, Neumann JHL, Hilgendorff A, Behr J, O'Reilly M, Lehmann M, Burgstaller G, Konigshoff M, Chapman HA, Theis FJ, Schiller HB. Alveolar regeneration through a Krt8+ transitional stem cell state that persists in human lung fibrosis. *Nat Commun* 2020: 11(1): 3559.
41. Browaeys R, Saelens W, Saeys Y. NicheNet: modeling intercellular communication by linking ligands to target genes. *Nat Methods* 2020: 17(2): 159-162.
42. Rafii S, Butler JM, Ding BS. Angiocrine functions of organ-specific endothelial cells. *Nature* 2016: 529(7586): 316-325.
43. Ricard N, Bailly S, Guignabert C, Simons M. The quiescent endothelium: signalling pathways regulating organ-specific endothelial normalcy. *Nat Rev Cardiol* 2021: 18(8): 565-580.
44. Xu S, Liu Y, Ding Y, Luo S, Zheng X, Wu X, Liu Z, Ilyas I, Chen S, Han S, Little PJ, Jain MK, Weng J. The zinc finger transcription factor, KLF2, protects against COVID-19 associated endothelial dysfunction. *Signal Transduct Target Ther* 2021: 6(1): 266.
45. Huang LT, Chang HW, Wu MJ, Lai YT, Wu WC, Yu WCY, Chang VHS. Klf10 deficiency in mice exacerbates pulmonary inflammation by increasing expression of the proinflammatory molecule NPRA. *Int J Biochem Cell Biol* 2016: 79: 231-238.
46. Malinverno M, Corada M, Ferrarini L, Formicola L, Marazzi G, Sassoon D, Dejana E. Peg3/PW1 Is a Marker of a Subset of Vessel Associated Endothelial Progenitors. *Stem Cells* 2017: 35(5): 1328-1340.
47. Zanini F, Che X, Knutsen C, Liu M, Suresh NE, Domingo-Gonzalez R, Dou SH, Zhang D, Pryhuber GS, Jones RC, Quake SR, Cornfield DN, Alvira CM. Developmental diversity and unique sensitivity to injury of lung endothelial subtypes during postnatal growth. *iScience* 2023: 26(3): 106097.
48. Habermann AC, Gutierrez AJ, Bui LT, Yahn SL, Winters NI, Calvi CL, Peter L, Chung MI, Taylor CJ, Jetter C, Raju L, Roberson J, Ding G, Wood L, Sucre JMS, Richmond BW, Serezani AP, McDonnell WJ, Mallal SB, Bacchetta MJ, Loyd JE, Shaver CM, Ware LB, Bremner R, Walia R, Blackwell TS, Banovich NE, Kropski JA. Single-cell RNA sequencing

reveals profibrotic roles of distinct epithelial and mesenchymal lineages in pulmonary fibrosis. *Sci Adv* 2020: 6(28): eaba1972.
49. Ono R, Kaisho T, Tanaka T. PDLIM1 inhibits NF-kappaB-mediated inflammatory signaling by sequestering the p65 subunit of NF-kappaB in the cytoplasm. *Sci Rep* 2015: 5: 18327.
50. Bergen V, Lange M, Peidli S, Wolf FA, Theis FJ. Generalizing RNA velocity to transient cell states through dynamical modeling. *Nat Biotechnol* 2020: 38(12): 1408-1414.
51. Sari E, He C, Margaroli C. Plasticity towards Rigidity: A Macrophage Conundrum in Pulmonary Fibrosis. *Int J Mol Sci* 2022: 23(19).
52. Camilli C, Hoeh AE, De Rossi G, Moss SE, Greenwood J. LRG1: an emerging player in disease pathogenesis. *J Biomed Sci* 2022: 29(1): 6.
53. Wang Y, Xu J, Zhang X, Wang C, Huang Y, Dai K, Zhang X. TNF-alpha-induced LRG1 promotes angiogenesis and mesenchymal stem cell migration in the subchondral bone during osteoarthritis. *Cell Death Dis* 2017: 8(3): e2715.
54. Hughes K, Wickenden JA, Allen JE, Watson CJ. Conditional deletion of Stat3 in mammary epithelium impairs the acute phase response and modulates immune cell numbers during post-lactational regression. *J Pathol* 2012: 227(1): 106-117.
55. Liu C, Lim ST, Teo MHY, Tan MSY, Kulkarni MD, Qiu B, Li A, Lal S, Dos Remedios CG, Tan NS, Wahli W, Ferenczi MA, Song W, Hong W, Wang X. Collaborative Regulation of LRG1 by TGF-beta1 and PPAR-beta/delta Modulates Chronic Pressure Overload-Induced Cardiac Fibrosis. *Circ Heart Fail* 2019: 12(12): e005962.
56. Sng MK, Chan JSK, Teo Z, Phua T, Tan EHP, Wee JWK, Koh NJN, Tan CK, Chen JP, Pal M, Tong BMK, Tnay YL, Ng XR, Zhu P, Chiba S, Wang X, Wahli W, Tan NS. Selective deletion of PPARbeta/delta in fibroblasts causes dermal fibrosis by attenuated LRG1 expression. *Cell Discov* 2018: 4: 15.
57. Honda H, Fujimoto M, Serada S, Urushima H, Mishima T, Lee H, Ohkawara T, Kohno N, Hattori N, Yokoyama A, Naka T. Leucine-rich alpha-2 glycoprotein promotes lung fibrosis by modulating TGF-beta signaling in fibroblasts. *Physiol Rep* 2017: 5(24).
58. Liu M, Zhang L, Marsboom G, Jambusaria A, Xiong S, Toth PT, Benevolenskaya EV, Rehman J, Malik AB. Sox17 is required for endothelial regeneration following inflammation-induced vascular injury. *Nat Commun* 2019: 10(1): 2126.
59. Krock BL, Skuli N, Simon MC. Hypoxia-induced angiogenesis: good and evil. *Genes Cancer* 2011: 2(12): 1117-1133.
60. Marsboom G, Rehman J. Hypoxia Signaling in Vascular Homeostasis. *Physiology (Bethesda)* 2018: 33(5): 328-337.
61. Amersfoort J, Eelen G, Carmeliet P. Immunomodulation by endothelial cells - partnering up with the immune system? *Nat Rev Immunol* 2022: 22(9): 576-588.
62. Mai J, Virtue A, Shen J, Wang H, Yang XF. An evolving new paradigm: endothelial cells--conditional innate immune cells. *J Hematol Oncol* 2013: 6: 61.
63. Kreisel D, Richardson SB, Li W, Lin X, Kornfeld CG, Sugimoto S, Hsieh CS, Gelman AE, Krupnick AS. Cutting edge: MHC class II expression by pulmonary nonhematopoietic cells plays a critical role in controlling local inflammatory responses. *J Immunol* 2010: 185(7): 3809-3813.
64. Goveia J, Rohlenova K, Taverna F, Treps L, Conradi LC, Pircher A, Geldhof V, de Rooij L, Kalucka J, Sokol L, Garcia-Caballero M, Zheng Y, Qian J, Teuwen LA, Khan S, Boeckx B, Wauters E, Decaluwe H, De Leyn P, Vansteenkiste J, Weynand B, Sagaert X, Verbeken E, Wolthuis A, Topal B, Everaerts W, Bohnenberger H, Emmert A, Panovska D, De Smet F, Staal FJT, McLaughlin RJ, Impens F, Lagani V, Vinckier S, Mazzone M, Schoonjans L, Dewerchin M, Eelen G, Karakach TK, Yang H, Wang J, Bolund L, Lin L, Thienpont B, Li X, Lambrechts D, Luo Y, Carmeliet P. An Integrated Gene Expression Landscape Profiling Approach to Identify Lung Tumor Endothelial Cell Heterogeneity and Angiogenic Candidates. *Cancer Cell* 2020: 37(1): 21-36 e13.
65. Angelidis I, Simon LM, Fernandez IE, Strunz M, Mayr CH, Greiffo FR, Tsitsiridis G, Ansari M, Graf E, Strom TM, Nagendran M, Desai T, Eickelberg O, Mann M, Theis FJ, Schiller HB. An atlas of the aging lung mapped by single cell transcriptomics and deep tissue proteomics. *Nat Commun* 2019: 10(1): 963.

66. Teuwen LA, Geldhof V, Pasut A, Carmeliet P. COVID-19: the vasculature unleashed. *Nat Rev Immunol* 2020: 20(7): 389-391.
67. Hoyne GF, Elliott H, Mutsaers SE, Prele CM. Idiopathic pulmonary fibrosis and a role for autoimmunity. *Immunol Cell Biol* 2017: 95(7): 577-583.
68. Heukels P, Moor CC, von der Thusen JH, Wijsenbeek MS, Kool M. Inflammation and immunity in IPF pathogenesis and treatment. *Respir Med* 2019: 147: 79-91.
69. Lang NJ, Gote-Schniering J, Porras-Gonzalez D, Yang L, De Sadeleer LJ, Jentzsch RC, Shitov VA, Zhou S, Ansari M, Agami A, Mayr CH, Kashani BH, Chen Y, Heumos L, Pestoni JC, Geeraerts E, Anquetil V, Saniere L, Wögrath M, Gerckens M, Hatz R, Kneidinger N, Behr J, Wuyts WA, Stoleriu M-G, Luecken MD, Theis FJ, Burgstaller G, Schiller HB. Ex vivo tissue perturbations coupled to single cell RNA-seq reveal multi-lineage cell circuit dynamics in human lung fibrogenesis. *bioRxiv* 2023.
70. Raslan AA, Pham TX, Lee J, Hong J, Schmottlach J, Nicolas K, Dinc T, Bujor AM, Caporarello N, Thiriot A, von Andrian UH, Huang SK, Nicosia RF, Trojanowska M, Varelas X, Ligresti G. Single Cell Transcriptomics of Fibrotic Lungs Unveils Aging-associated Alterations in Endothelial and Epithelial Cell Regeneration. *bioRxiv* 2023.
71. Savary G, Dewaeles E, Diazzi S, Buscot M, Nottet N, Fassy J, Courcot E, Henaoui IS, Lemaire J, Martis N, Van der Hauwaert C, Pons N, Magnone V, Leroy S, Hofman V, Plantier L, Lebrigand K, Paquet A, Lino Cardenas CL, Vassaux G, Hofman P, Gunther A, Crestani B, Wallaert B, Rezzonico R, Brousseau T, Glowacki F, Bellusci S, Perrais M, Broly F, Barbry P, Marquette CH, Cauffiez C, Mari B, Pottier N. The Long Non-Coding RNA DNM3OS is a Reservoir of FibromiRs with Major Functions in Lung Fibroblast Response to TGF-beta and Pulmonary Fibrosis. *Am J Respir Crit Care Med* 2019.